LAWRENCE
LIVERMORE
NATIONAL
LABORATORY

LLNL-JRNL-655965

Ensemble Simulations of the Role of the Stratosphere in the Attribution of Tropospheric Ozone Variability

P. G. Hess, D. Kinnison, Q. Tang

June 18, 2014

Atmospheric Chemistry and Physics

Disclaimer

LLNL-JRNL-655965

Ensemble Simulations of the Role of the Stratosphere in the Attribution of Tropospheric Ozone Variability

Peter Hess[1], Doug Kinnison[2], Qi Tang[3]
1 Cornell University, Ithaca, NY, USA, pgh25@cornell.edu
2 National Center for Atmospheric Research, Boulder, CO, USA
3 Lawrence Livermore National Laboratory, Livermore, CA, USA

Abstract:

Despite the need to understand the impact of changes in emissions and climate on tropospheric ozone, attribution of tropospheric interannual ozone variability to specific processes has proved difficult. Here we analyze the stratospheric contribution to tropospheric ozone variability and trends from 1953-2005 in the Northern Hemisphere (N.H.) mid-latitudes using four ensemble simulations of the Free Running (FR) Whole Atmosphere Community Climate Model (WACCM). The simulations are forced with observed time varying: (1) sea surface temperatures (SSTs), (2) greenhouse gases (GHGs), (3) ozone depleting substances (ODS), (4) Quasi-Biennial Oscillation (QBO); (5) solar variability (SV) and (6) stratospheric sulfate surface area density (SAD). Detailed representation of stratospheric chemistry is simulated including the ozone loss processes due to volcanic eruptions and polar stratospheric clouds. In the troposphere ozone production is represented by CH_4-NO_X smog chemistry, where surface chemical emissions remain interannually constant. Despite the simplicity of the tropospheric chemistry, the FR WACCM simulations capture the measured N.H. background interannual tropospheric ozone variability in many locations to a surprising extent, suggesting the importance of external forcing in driving interannual ozone variability. The variability and trend in the simulated 1953-2005 tropospheric ozone record from 30-90^o N at background surface measurement sites, 500 hPa measurement sites and in the area average is largely explained on interannual timescales by changes in the 150 hPa 30-90^o N ozone flux and changes in tropospheric methane concentrations. The average sensitivity of tropospheric ozone to methane (percent change in ozone to a percent change in methane) from 30-90^o N is 0.17 at 500 hPa and 0.21 at the surface; the average sensitivity of tropospheric ozone to the 150 hPa ozone flux (percent change in ozone to a percent change in the ozone flux) from 30-90^o N is 0.19 at 500 hPa and 0.11 at the surface. The 30-90^o N simulated downward residual velocity at 150 hPa increased by 15% between 1953 and 2005. However, the impact of this on the 30-90^o N 150 hPa ozone flux is modulated by the long-term changes in stratospheric ozone. The ozone flux decreases from 1965 to 1990 due to stratospheric ozone depletion, but increases again by approximately 7% from 1990-2005. The first empirical orthogonal function of interannual ozone variability explains from 40% (at the surface) to over 80% (at 150 hPa) of the simulated ozone variability from 30-90^o N. This identified mode of ozone variability shows strong stratosphere-troposphere coupling, demonstrating the importance of the stratosphere in an attribution of tropospheric ozone variability. The simulations, with no change in emissions, capture almost 50% of the measured ozone change during the 1990s at a variety of locations. This suggests that a large portion of the measured change is not due to changes in emissions, but can be traced to changes in large-scale modes of ozone variability. This emphasizes the difficulty in the attribution of ozone changes, and the importance of natural variability in understanding the trends and variability of ozone. We find little relation between the El Nino Southern Oscillation (ENSO) index and large-scale tropospheric ozone variability over the long-term record.

1. Introduction.

Global change will impact both tropospheric and stratospheric ozone concentrations. Ozone acts as a potent oxidant deleterious to human health, ecosystem and agricultural productivity; it shields the Earth's surface from harmful ultraviolet radiation; it is a greenhouse gas itself, and through its complex photochemistry regulates the lifetime of other greenhouse gases. Because of tropospheric ozone's importance as a surface pollutant the emissions of ozone precursors are regulated in many countries while the Montreal Protocol and its amendments regulate emitted species that act to destroy stratospheric ozone. To assess the impact of emission strategies in modifying atmospheric ozone there is a need to establish clear links between measured changes in ozone and the processes that cause these changes including changes in climate and changes in emissions. Using long-term global simulations of stratospheric and tropospheric ozone chemistry this paper demonstrates the large-scale coupling between extratropical tropospheric and stratospheric ozone variability. We show that an interpretation of interannual tropospheric ozone variability must account for changes in stratosphere-to-troposphere exchange (STE) of ozone.

The tropospheric ozone budget can be summarized in terms of photochemical ozone production and loss, the input of ozone from the stratosphere and the loss of ozone due to surface deposition. The largest terms, the photochemical production and loss of ozone nearly balance each other [*Stevenson et al.*, 2006]. Surface ozone deposition and influx from the stratosphere are each larger than the net photochemistry [*Stevenson et al.*, 2006]. Changes in the influx of ozone from the stratosphere to the troposphere are buffered by compensating changes in tropospheric photochemical ozone loss and surface deposition [*Hess and Zbinden*, 2013; *Tang et al.*, 2013; *Zeng and Pyle*, 2005]. Future increases in the exchange of ozone from the stratosphere to troposphere are predicted with impacts on tropospheric ozone [*Stevenson et al.*, 2006; *Collins et al.*, 2003; *Zeng and Pyle*, 2003; *Shindell et al.*, 2006; *Hegglin and Shepherd*, 2009].

Except in association with particular events an overall attribution of tropospheric interannual ozone variability to specific processes has proved difficult. While very long-term ozone increases since the preindustrial are generally attributed to changes in emissions, simulations tend to underestimate the overall century time-scale ozone increases [e.g., *Lamarque et al.*, 2005; *Mickley et al.*, 2001] as estimated from the semi-quantitative ozone measurements at the end of the 19th century [*Volz and Kley*, 1988; *Marenco et al.*, 1994]. Even on the multidecadal timescales since the advent of more modern measurement techniques an attribution of measured tropospheric trends has proved difficult: the extent of the ozone increase since the 1960s as inferred from long-term N.H. measurements has not been simulated [*Lamarque et al.*, 2010; *Parrish et al.*, 2014].

Lin et al. [2014] attributes decadal changes in the interannual Mauna Loa ozone record to shifts in circulation patterns. However, in other locations ozone exhibits considerable interannual variability on decadal timescales that has not been adequately explained [e.g., *Koumoutsaris et al.*, 2008]. In many cases this ozone variability is not easily ascribed to

changes in emissions. For example, changes in emissions do not explain the ozone trends at Mace Head, Ireland [e.g., *Hess and Zbinden*, 2013; *Fiore et al.*, 2009], measured as strongly positive during the most of the 1990s but since leveling off [*Simmonds et al.*, 2004; *Carslaw*, 2005; *Derwent et al.*, 2007]. In an analysis of ozone trends over Europe *Wilson et al.* [2012] conclude the impact of European precursor emission reductions were masked by other sources of unknown ozone variability. Analysis by *Logan et al.* [2012] and *Cui et al.* [2011] suggest the measured ozone increases at alpine sites over Europe during the 1990s followed by decreases after 2000 are not easily explained by changes in emissions or changes in lower stratospheric ozone. *Pozzoli et al.* [2011] conclude that changes in meteorology and natural emissions account for 75% of ozone variability from 1980-2005, largely masking changes in anthropogenic emissions. On decadal timescales ozone trends can depend sensitively on the exact time-period examined [*Cui et al.*, 2011].

While an overall attribution and synthesis of tropospheric ozone variability may be lacking, sources of variability associated with various events have been isolated. The analysis of *Leibensperger et al.* [2008] shows that decadal and interannual cyclone trends have important impacts on surface ozone variability and trends over the North East US, although the analysis of *Turner et al.* [2013] suggests cyclones explain less than 10% of the overall variability of high ozone events over this region. Over the Eastern half of the US changes in interannual temperatures explain between approximately 25-50% of the interannual regional ozone variability in July, although changes in temperature mask many other processes. *Jaffe et al.* [2008] associates interannual variability in ozone across the Western U.S. with biomass burning. Interannual variability in ozone due to changes in emissions and due to heat waves (sometimes also associated with changes in emissions) has also been shown to be important [*Tressol et al.*, 2008; *Konovalov et al.*, 2011].

It is well known that stratospheric ozone can be transported into the troposphere [e.g., *Danielsen*, 1968]. Vertical correlations between stratospheric and tropospheric ozone have been analyzed in measurements [*Hess and Zbinden*, 2013; *Tarasick*, 2005; *Thouret et al.*, 2006; *Ordóñez et al.*, 2007, *Neu et al.* 2014] and in a model simulations [*Terao et al.*, 2008, *Hess and Zbinden*, 2013]. A number of modeling studies have attributed extratropical N.H. tropospheric ozone variability to El Nino Southern Oscillation (ENSO) [*Zeng and Pyle*, 2005; *Doherty et al.*, 2006; *Koumoutsaris et al.*, 2008; *Voulgarakis et al.*, 2011] modulated through STE [*Zeng and Pyle*, 2005; *Voulgarakis et al.*, 2011]. *Langford et al.* [1998] show the modulation of middle and upper tropospheric ozone due to ENSO using LIDAR measurements over Colorado. They suggest that this modulation may induce different long-term decadal ozone trends (between −0.2 to +0.5 ppbv/yr) depending on the exact period the ozone trend is examined. On the other hand, *Hsu and Prather* [2009] do not find a relationship between ENSO and STE. Other studies have attributed ozone variability to the North Atlantic Oscillation (NAO) or Artic Oscillation (AO) [*Li*, 2002; *Creilson et al.*, 2003, 2005; *Lamarque and Hess*, 2003; *Hess and Lamarque*, 2007; *Sprenger*, 2003; *Pausata et al.*, 2012] with associated changes in STE [*Sprenger*, 2003; *Hess and Lamarque*, 2007]. *Hsu and Prather* [2009] show considerable interannual variability in stratosphere-troposphere exchange and attribute 20-40% of this variability to the quasi-biennial oscillation (QBO). Tropospheric ozone decreases have

been simulated following the Mt Pinatubo eruption due to changes in STE [*Tang et al.*, 2013]. *Hess and Zbinden* [2013] argue that to a significant extent interannual variability in extratropical tropospheric ozone is due to the variability in ozone transported from stratosphere. *Neu et al.* [2014] attribute approximately half of tropospheric ozone variability to interannual changes in the strength of the stratospheric circulation.

In this paper we use a synthesis of simulations and measurements to demonstrate the importance of large-scale coupled stratosphere-troposphere modes in determining tropospheric ozone variability from 30-90^{o} N. These results are an extension and expansion of the simulations analyzed in *Hess and Zbinden* [2013], who showed the importance of stratosphere-troposphere exchange in explaining N.H. extratropical tropospheric ozone variability from 1990-2006. We expand on the work of *Hess and Zbinden* [2013] by: (1) using simulations with good stratospheric resolution and detailed representation of stratospheric chemistry incorporating the impacts of interannual changes in stratospheric aerosol loading and ozone depleting substances (ODS). (2) Simulating the chemical coupling between the stratosphere and troposphere over a period of more than 50 years (1953-2005), a period incorporating the rapid growth and then decline of the emissions of ODS. (3) Analyzing the extent to which the coupled variability of the lower stratosphere and tropospheric ozone is externally (e.g., by changes in sea surface temperatures) versus internally forced. (4) Incorporating further analysis of the large scale coupled modes linking stratospheric and tropospheric ozone variability.

Distinct from *Hess and Zbinden* [2013] we use a simulation that only simulates basic tropospheric NOx-CH4 chemistry. By examining the importance of stratospheric-tropospheric coupling using a basic set of tropospheric chemistry reactions, the importance of more complex chemistry in determining tropospheric ozone variability can be better understood. It is expected that the introduction of additional hydrocarbon chemistry as well as episodic emission variability (e.g., biomass burning) will introduce additional modes of variability not captured here. In addition more complex chemistry may possibly dampen the basic modes of ozone variability described below. However, despite the simplicity in the tropospheric chemistry, these simulations match the observed variability to a large extent. Thus we view the modes of ozone variability captured here as base-state modes which may be perturbed by more complex chemistry, but are fundamental to the coupled troposphere-stratosphere chemical system.

The model description and description of the data analyzed is given in section 2. An evaluation of the simulations is given in section 3. Section 4 analyzes the ozone variability. Discussion and conclusions are given in Section 5.

2. Methodology

2.1 Model Description

The Whole-Atmosphere Community Climate Model, Version 3.5 (WACCM3) is a comprehensive numerical model simulating the dynamics and chemistry of the atmosphere, spanning the range of altitude from the Earth's surface to the lower thermosphere. WACCM3 is a fully interactive model, wherein the radiatively active gases (CO_2, H_2O, N_2O, CH_4, CFC-11, CFC-12, NO, O_3) affect heating and cooling rates and therefore dynamics [*Sassi et al*., 2005]. WACCM is based on the software framework of the Community Atmospheric Model (CAM). WACCM3, is a superset of CAM version 3 (CAM3), and includes all of the physical parameterizations of that model. A finite volume dynamical core [*Lin*, 2004], which is an option in CAM3, is used exclusively in WACCM3. This numerical method calculates explicitly the mass fluxes in and out of a given model grid cell, thus ensuring mass conservation.

The governing equations, physical parameterizations and numerical algorithms used in CAM3 are documented by *Collins et al*. [2004]; only the gravity wave drag and vertical diffusion parameterizations are modified for WACCM3. In addition, WACCM3 incorporates a detailed neutral chemistry model for the middle atmosphere, including heating due to chemical reactions; a model of ion chemistry in the mesosphere / lower thermosphere (M/LT); ion drag and auroral processes; and parameterizations of short wave heating at extreme ultraviolet (EUV) wavelengths and infrared transfer under non-local thermodynamic equilibrium (NLTE) conditions. Processes and parameterizations that are unique to WACCM3 are discussed in *Garcia et al*. [2007]; for other details, the reader is referred to the papers of *Collins et al*. [2004].

The chemistry module is based on the Model for OZone And Related chemical Tracers version 3 (MOZART3) [*Kinnison et al.,* 2007]. The species included within this mechanism are contained within the O_X, NO_X, HO_X, ClO_X, and BrO_X chemical families, along with CH_4 and its degradation products (a total of 59 species and 217 gas-phase chemical reactions). This chemical mechanism includes 10 long-lived organic halogens (i.e., CH_3Cl, CFC-11, CFC-12, CFC-113, HCFC-22, CCl_4, CH_3CCl_3, halon-1211, halon-1301, and CH_3Br). Rate constants are based on *Sander et al.* [2006]. In addition, there are 17 heterogeneous reactions on three aerosol types: Nitric Acid Trihydrate (NAT), Supercooled Ternary Solution (STS), and Water-Ice. A detailed description of the chemical approach can be found in *Kinnison et al.* [2007].

For this work, the Chemistry Climate Model Validation Activity for SPARC, version 2 (CCMVal2) REF1 scenario was used (see *Eyring et al*., 2008). This scenario included observed time-dependent evolution of: greenhouse gases (GHGs); ozone depleting substances (ODSs); sea surface temperatures and sea ice concentrations (SSTs/SICs); stratospheric sulfate surface area densities (SADs); 11-year solar cycle variability, which includes spectrally resolved solar irradiances; Quasi-Biennial Oscillation (QBO), by relaxing to observed tropical winds. Surface emissions of CO, NO_X, and formaldehyde are included but the emission trends are not simulated. The emissions are set to present day conditions. This version of WACCM was extensively evaluated in the SPARC Report of

231 the Evaluation of Chemistry-Climate Models [*SPARC*, 2010]. Four long-term ensemble
232 simulations (1953-2005) are analyzed here focusing on the tropospheric and lower
233 stratospheric ozone distribution from 30-90^{o} N.
234
235 Figure 1 gives the change in boundary conditions for CH_4 and CFC-11. CFC-11 peaks in
236 1992 [*World Meteorological Organization (WMO),* 2007] and then begins to slowly
237 decline. Methane shows a nonlinear growth rate with evidence of a flattening in the trend
238 beginning in the early 1990s [e.g., *Dlugokencky et al.*, 2011].
239
240 **2.2 Data**
241
242 The WACCM simulation is evaluated at 150 hPa, 500 hPa, and a number of surface
243 stations between 30 and 90^{o} N including elevated alpine sites. Long-term monitoring
244 sites and ozonesonde records are used for model evaluation (see Table 1).
245
246 Ozonesonde data is obtained from the World Ozone and Ultraviolet Radiation Data
247 Centre (WOUDC). The methodology for filtering the measurements is similar to that
248 described in *Hess and Zbinden* [2013] except we combined different measurement
249 techniques together so as to extend the measurement records as far back as possible. As
250 in *Hess and Zbinden* [2013]we aggregated the 150 and 500 hPa ozonesonde data into
251 geographical regions. This acts to isolate the larger-scale interannual variability and
252 increases the sampling frequency. We use geographical regions located between 30 and
253 90^{o} N where at least two long-term independent ozonesonde measurements are available:
254 Canada, Central Europe, Japan and Northern Europe (see Table 1). Here we simply
255 aggregate the regional ozone measurements by averaging the individual measurements
256 within each region. *Hess and Zbinden* [2013] aggregated the measurements by averaging
257 their relative variability, but the two methodologies produce very similar results.
258
259 At the surface, we include many of the same long-term measurement sites between 30^{o}
260 and 90^{o} N as used in *Lamarque et al.* [2010] (see Table 1). We have combined the
261 Zugspitze alpine measurements with those of the neighboring Jungfraujoch surface
262 measurement site. We have omitted measurement sites immediately downwind of Asian
263 or U.S. emissions (Mt Happo, Japan; Bermuda; Sable Island, Novia Scotia) as our
264 simulations are best suited to sampling background air as we include no changes in
265 surface emissions. We have, however, included the Lassen National Park site in the
266 Western U.S. even though this site likely registers impacts of increasing Asian emissions
267 [e.g., *Parrish et al.*, 2012]. This site is subject to significant interannual variability not
268 explained by changes in Asian emissions (see Figure 6). We have also omitted the
269 Barrow site due to the influence of Arctic depletion events on the Barrow record [e.g.,
270 *Oltmans et al.*, 2012].
271
272 For each measurement site, or measurement region, monthly ozone deviations are
273 calculated as deviations from the monthly-averaged ozone distribution from January 1990
274 – December 2004. The monthly deviations are averaged using 12-month smoothing.
275
276 **3. Model Evaluation**

3.1 Ensemble Simulation Overview

Ozone for the four ensembles simulations averaged from 30-90^{o} N is shown in Figure 2 at 150, 500 and 1000 hPa. At each level for each of the ensemble simulations ozone follows a similar long-term trajectory. At 150 hPa this trajectory is at least partially governed by the ODS forcing common to all ensemble members. At 150 hPa, in the long-term average, ozone levels remain nearly constant until 1970, but thereafter decrease and reach a minimum between 1991 and 1994 in association with the Mt Pinatubo eruption. Note that even though all ensemble members simulate the ozone loss associated with Mt Pinatubo, the timing of this loss is partially governed by the internal model variability. In all simulations 150 hPa ozone partially recovers following the Mt Pinatubo period. At 500 hPa and the surface all simulations show a long-term ozone increase throughout the period. This increase can be largely attributed to the long-term methane forcing (Figure 1). The long-term growth in ozone is nearly continuous until approximately 1980 when it begins to flatten.

On shorter timescales each of the ensemble simulations follows its own path relative to the mean long-term trend. However, there are some notable periods where all ensemble members show similar behavior with a coincident ozone maximum or minimum across all model levels (e.g., 1965, 1967, 1972, 1973, 1998); during other periods the short timescale behavior of the individual the ensemble members appear unrelated (e.g., 1968-1971, 1977-1983, 1993-1997). In the sections below the model behavior depicted in Figure 2 is examined in detail. In this section the model measurement evaluation is given at selected sites from 150 hPa to the surface (see Table 1).

3.2 Model Evaluation

The model-measurement evaluation is shown Figures 3-6, in supplemental Figures 1-6 and is summarized in Table 2. A comparison of the area averaged ozone evolution (Figure 2) and that at the individual ozone sites reveals broad similarities. The similarity between the ozone evolution at various measurement sites and the overall hemispheric evolution was pointed out in *Hess and Zbinden* [2013]. This is further examined in section 4 where we examine coupled stratospheric-tropospheric modes of ozone variability.

The model-measurement correlations (Table 2) are between 12-month smoothed datasets and use detrended data so as not to introduce positive correlations simply through a simulation of long-term trends. In the stratosphere ozone is simply detrended against time; in the troposphere ozone is detrended against methane as changes in methane largely drive the simulated ozone increases (see section 4). We note it is difficult to unambiguously separate out the shorter term interannual variations from the longer term trends, particularly when the long-term trends have a comparable magnitude to the interannual variations. We believe this is particularly problematic in the analysis of some of the tropospheric measurements with large ozone increases (e.g., at Lassen). The model-measurement correlation is broken into two periods: prior to 1990 and subsequent

to 1990. The number of measurement sites and the increase in measurement accuracy make comparisons after 1990 particularly valuable. The model and measured record are only correlated when the records extend for periods of greater than five years. Shorter-term model-measurement comparisons (1991-1995) are made in *Tang et al.* [2013] using a similar formulation of WACCM as used here, but with full hydrocarbon chemistry in the troposphere. *Tang et al.* [2013] also compare the measurements against simulations using a specified dynamics formulation of WACCM, where WACCM is nudged to analyzed winds. The more tropospherically configured model, the Community Atmospheric Model with chemistry (CAM-chem) [*Lamarque et al.*, 2012] has been compared against a similar set of measurements in *Hess and Zbinden* [2013] and *Tang et al.* [2013].

Not until the early 1970s do ozonesonde measurements become available for the Canadian, Central European and Japanese sites (Table 2). Data is not available for the Northern European Region until the late 1980s. Each figure shows the observational record for each site within each region and documents the changes in the type of ozonesonde used at each site. The accuracy of the regionally averaged ozone records likely change with time as number of stations and measurement techniques change (e.g., from Brewer Mast (BM) ozonesondes to electrochemical concentration cells (ECC)). The standard deviation between the regional measurements shown at the bottom of each figure gives an indication of temporal changes in the regional consistency of the measurements.

3.2.1 150 hPa evaluation.

At 150 hPa simulated ozone remains fairly flat at the analyzed sites (e.g., Figure 3 and Figure S1-S3) until the early 1970s when the earliest measurements become available. Coincident with the increase in the concentrations of ODS (e.g., see Figure 1) simulated ozone decreases from the 1970s until the early 1990s over the four regions examined (Canada, Central Europe, Japan and Northern Europe). Measured decreases during this period are particularly notable over the Canadian and Central European regions. While the standard deviation between the regional measurement sites is comparatively large prior to 1990 over the Canadian region (Figure 3), the standard deviation is still smaller than the overall long-term trend (1970-1990). The early record over Japan is somewhat noiser, but also suggests long-term ozone decreases during this period (Figure S2). The negative ozone deviations at 150 hPa in the early 1990s can be attributed to Mt Pinatubo, which resulted in significant ozone depletion in the northern mid-latitudes beginning in 1991 and lasting through 1995 [*Tang et al.*, 2013]. Since the early 1990s the 150 hPa ozone at the evaluated sites has recovered to some extent.

In addition to the long-term trends the simulations and measurements also exhibit considerable shorter-term interannual variability at 150 hPa. For the period beginning in 1990 the model and measured records are significantly correlated over Canada and Northern Europe (Figure 3, Figure S3, Table 2). For example after 1990 both measurements and simulated ozone over Canada and Northern Europe have an ozone minimum during the Mt Pinatubo period, a maximum in 1998–1999 and 2002-2003 and

pronounced ozone minima near 2000. These features can also be seen in the Central European record (Figure S1). Prior to 1990 the detrended simulated and measured variability are significantly correlated over Canada and Central Europe (Table 2) at 150 hPa. Over Canada the standard deviation between the individual station measurements increases substantially prior to 1990, suggesting caution in interpreting the early measurements. Nevertheless, the peak in the Canadian measurements in 1970 and 1973 and the broad peak from 1977-1983 correspond to similar features in the Central European measurements suggesting that these features may be real. The simulation and measurements are not significantly correlated over Japan. *Hess and Zbinden* [2013] found the measurements between the individual stations over Japan did not exhibit temporal coherence. This is evident from the rather high standard deviation between the ozonesonde stations (Figure S2). In fact we have not been able to simulate the ozone record over Japan either prior to 1990 or subsequent to 1990 at either 150 hPa or at 500 hPa in the current simulations.

3.2.2 500 hPa evaluation

While the 150 hPa simulated and measured standard deviation between regional sites was similar in the model and measurements (Figure 3, Figure S1-S3), at 500 hPa the measured standard deviation is much larger than that simulated (Figure 4, S4, S5). This suggests a comparative degradation in the measurement accuracy at 500 hPa compared to 150 hPa and/or geographical variability not simulated. Over Europe in particular, the measured standard deviation increases significantly prior to 1990. The analysis of *Logan et al.* [2012] suggests the ozonesonde data has only been coherent over Europe since 1998. *Hess and Zbinden* [2013] also noted discrepancies in the European data during the 1990s.

Over the long-term significant ozone increases are both simulated and measured over the 500 hPa tropospheric sites. In the simulation these increases can be attributed to the long-term increases in methane (Figure 1); in the measurements, the emissions of many other ozone precursors also increased over this time period. Prior to the early 1980s simulated ozone significantly over predicts the tropospheric measurements, except over Japan. We note that even simulations using complex mechanisms for tropospheric photochemistry and time varying emission inventories have not been able to capture the measured ozone increases [*Lamarque et al.*, 2010; *Parrish et al.*, 2014]. The Canadian sites show a rapid ozone increase until 1980, while the Central European sites show this increase lasts until the middle to late 1980s, consistent with European Alpine sites (see Figure 5). However, whereas the Canadian and alpine sites suggest ozone in the mid-1980s was comparable to the concentrations after 2000, the Central European ozonesondes show much elevated concentrations during this earlier period. The measured high ozone concentrations over Central Europe at 500 hPa are not simulated.

Except over Japan the model and measurements are significantly correlated after 1990 at 500 hPa over the evaluated regions (Table 2). During the early 1990s the eruption of Mt Pinatubo resulted in anomalously low tropospheric ozone [*Tang et al.*, 2013] clearly evident over the Central and Northern European and Canadian regions in both the

simulations and measurements (Figures 4, S4). The elevated ozone in 1998-1999 evident in the measurements and simulations [also see *Thouret et al.*, 2006; *Zbinden et al.*, 2006] has been attributed to ENSO [*Koumoutsaris et al.*, 2008; *Voulgarakis et al.*, 2011] and is has been associated with increases in STE ([*Voulgarakis et al.*, 2011, *Hess and Zbinden* 2013]). The model and measurements are also significantly correlated over the Canadian ozonesonde sites prior to 1990.

3.2.3 Surface Sites

As at 500 hPa, the European Mountain sites (Figure 5), the Mt Lassen site in California (Figure 6), the Arkona site in Continental Europe (Figure S6) and the Mace Head site in Western Europe (Figure 5) all exhibit an ozone minimum in the measurements and simulations near 1993-1994 (although not very pronounced in the Mace Head measurements) and an ozone maximum near1998-1999. The simulations and measurements are significantly correlated at the European mountain sites after 1990 (Figures 5a) and at Mace Head (Figure 5b), but not at Lassen (Figure 6) or Arkona (Figure S6). The Lassen site in California sites is susceptible to the ozone increases attributable to the large increase in Asian ozone precursor emissions [e.g., *Cooper et al.*, 2010], increases not included in the simulation. Interannual variability in the transport of ozone produced from these Asian emissions as well difficulties in unambiguously removing the ozone trend at Lassen may contribute to the low model-measurement correlation at that site. Measured ozone increases between the 1993-1994 ozone minimum and the 1998-1999 ozone maximum are 5.7 ppb over the European Alpine sites, 6.6 ppb at Mace Head and 8.0 ppb at Lassen. The respective simulated ozone increases are 3.4 ppb, 4.0 ppb and 3.5 ppb or 60%, 61% and 44% of the measured increases. The model simulations, assuming no increases in emissions capture much of the measured variability and ozone change that occurred since 1990 at the these sites. The Arkona site is situated over continental Europe in a region immediately impacted by European emissions. At this site the simulations dramatically over estimate the measured concentrations prior to 1990 (Figure S6) and do not capture the ozone variability subsequent to 1990.

4 Long-term Tropospheric Ozone Variability

4.1 Forced vs. Unforced Variability

Over the long-term the trends in the simulated and measured ozone are driven by the trends in the concentrations of ODSs and methane and the solar cycle. Short-term external forcing can be attributed to forcing by sea surface temperature, volcanoes and the QBO. To the extent that the ozone record is driven by internal model dynamics versus external forcing we would expect the ozone records from the different ensemble members to be uncorrelated with each other and uncorrelated with the measurements. Given a perfect model (and perfect measurements) the correlation between simulations and measurements should give an indication of the importance of external forcing to the simulations. However, the detrended correlation between simulations and measurements is notable (Table 2), particularly for the period after 1990. The positive and significant

model-measurement correlation, in simulations in which model dynamics is internally calculated, emphasizes the importance of forced variability in driving the ozone variations.

The correlation between ensemble members also provides an indication of the extent to which the model is externally forced. The average median detrended correlation between the different simulations at all sites is highly significant (see Table 2), suggesting the role of external forcing is significant. These correlations tend to be somewhat lower at the surface. They are lowest at Arkona suggesting a decreased role for forced variability in association with high surface emissions. The ensemble correlations suggest that between 6 and 19% of the surface ozone variability at the surface measurement sites can be explained by external forcing and between 16 and 25% of the variability is forced at 500 and 150 hPa. The ensemble correlations over the course of the simulation are generally less than the model-measurement correlations, but the high model-measurement correlations generally occur after 1990 when the external forcing due to Mt Pinatubo and the 1998-1999 El Nino is particularly strong.

4.2 Response of tropospheric ozone to changes in methane and stratospheric ozone flux

In addition to photochemical changes in the tropospheric ozone budget, tropospheric ozone is modulated by the flux of ozone from the stratosphere [e.g., *Stevenson et al.*, 2006]. The vertical component of the zonally averaged vertical residual velocity ($\overline{w}^*$) and the ozone flux across150 hPa averaged from 30-90^o N is shown in Figure 7 for each ensemble member. The vertical component of the residual circulation ($\overline{w}^*$) approximates the vertical transport circulation [*Andrews et al.*, 1987] and serves as a measure of the strength of the overturning Brewer and Dobson circulation. The averaged downward residual velocity at 150 hPa increases from 1953-2005 (Figure 7a) in all the ensemble simulations. We note during some years $\overline{w}^*$ in each of the ensemble simulations is similar, while during other years $\overline{w}^*$ appears rather unrelated between the different ensembles. On average the residual circulation increases downward by approximately 15% over the course of the simulation. This increase in the residual circulation is a robust feature of chemistry climate model simulations [*Butchart et al.,* 2006, 2010; *Eyring et al.*, 2010a; *Oman et al.*, 2010; *Eyring et al.*, 2010b]. A cubic fit (Figure 7) suggests this increase is not exactly linear, but has increased since 1990.

The 150 hPa ozone flux averaged from 30-90^o N is calculated by multiplying the residual vertical velocity by the ozone concentration. *Gettleman et al.* [1997] suggests that the flux of ozone across this level serves as a good proxy for the flux of ozone from the stratosphere to the troposphere. While diagnostics of the STE of ozone across the tropopause would be preferable, it could not be estimated precisely from the monthly averaged model output fields saved from these simulations. In contrast to the fitted increase in the downwards-residual velocity (Figure 7a), the change in the ozone flux has not been monotonic (Figure 7b). The cubic fit to the ozone flux reaches a maximum in the 1960s as the residual circulation increases in strength and stratospheric ozone remains fairly constant; following this period the ozone flux decreases until the early 1990s (corresponding to the time of the Mt. Pinatubo eruption) as stratospheric ozone decreases;

following Mt Pinatubo the ozone flux increases again until the end of the model simulation. On average the ozone flux has increased by 8% from 1953-2005, about half the rate of increase of the residual circulation. *Hegglin and Shepherd* [2009] also show the ozone flux is modulated by ozone depletion in the N.H., but suggest no long-term decrease in the flux with the smallest fluxes occurring near 2000. We note the simulations described in *Hegglin and Shepherd* [2009] include no forcing due to volcanoes. In the future, predicted stratospheric ozone recovery and predicted increases in the strength of the residual circulation are expected to lead to further increases in the stratosphere-to-troposphere exchange of ozone [e.g., *Hegglin and Shepherd*, 2009].

The long-term impact of changes in the stratospheric ozone flux on tropospheric ozone is clearly seen in Figure 8. Here we examine the evolution of normalized ozone against tropospheric methane. Ozone is normalized by dividing the ozone record by the average ozone concentration from 1980-1985: *Parrish et al.* [2014] found that normalizing ozone helped reduced the ozone record at different measurement sites to a common curve. The exact date used for normalization is arbitrary. We found the data displayed nicely when we used the average value from 1980-1985 to normalize the ozone record. The simulated record of normalized ozone plotted against globally averaged methane reduces the ozone record to a set of similar curves at various tropospheric measurement sites (Figure 8a). We find that a cubit fit captures some of the subtleties of the long-term record better than a quadratic fit. Discussion of various polynomial fits is given in *Parrish et al.* [2014]. Here we only display those locations (see Table 1) where the ozone measurements extend to the early 1980s.

The long-term cubic fit to simulated ozone is not linear with respect to methane. Instead, at all sites, the simulated ozone increase with respect to methane is relatively fast between approximately 1953-1970 and 1990-2005, but is noticeably slower from 1970 to 1990. As the simulated surface NO_X emissions are not increasing over the course of the simulation, we would expect the ozone production from the simulated methane NO_X tropospheric chemistry to be approximately linear in methane. The simulated long-term non-linearity in ozone with respect to methane is consistent with the long-term modulations in the flux of ozone from the stratosphere: the period of slow tropospheric ozone growth (from approximately 1970-1990) is coincident with the decrease in the flux of ozone from the stratosphere.

It is difficult to draw any strong conclusions through a comparison of the simulated and measured ozone-methane curves (Fig. 8). The measured curves show a variety of different shapes. The measured curve over Central Europe reaches a maximum near 1990 and then decreases. This curve is undoubtedly impacted by the high measured ozone concentrations over Central Europe in the 1980s (Figure 4). These early measurements should be treated with caution. The Japanese measurements also suggest an early ozone maximum (in the 1980s), but show an ozone increase in the latest period. Other measured curves show an ozone increase near the end of the period. The cubic fit to the data is likely sensitive to the length of the data record as well as to the ends of the measured record.

In the measured curves it is difficult, if not impossible, to separate out the impact of changes in the emissions of ozone precursors from that due to changes in the influx of ozone from the stratosphere. If, for example, we concentrate on changes in the emissions of NO_X, the emissions increased rapidly in Europe from 1950-1980 by approximately 500% [*Vestreng et al.*, 2009], flattened out between 1980 and 1990 and decreased thereafter. The U.S. emissions stabilized following the clean air act of 1970 [*Office of Air Quality Planning and Standards*] after increasing by approximately 250% from 1950 - 1970. Emissions over East Asia increased by approximately 250% between 1980 and 2000, but were not commensurate with either US or European emissions until approximately 1995 [*Ohara et al.*, 2007]. Since the simulation does not include these changes in ozone precursor emissions it is not surprising that measured ozone changes (Figure 8) are about a factor of three to four larger than those simulated. The measured sharp increase in ozone prior to 1970-1980 and then the transition to a flatter trend is consistent with the emission changes. After 1985 the shape of the various measured curves is not consistent.

The coefficients for the multiple regression of simulated normalized ozone against normalized methane and the normalized stratospheric 150 hPa ozone flux (averaged from 30-90^o N) are given in Table 3 at various measurement sites and for the 30-90^o N area-averaged ozone. In this regression we average across the four ensemble members. The best fit is obtained when the tropospheric response lags the ozone flux by approximately 5-6 months. At all sites correlations between the regressed fit and the simulated ozone are highly significant and greater than 0.9 (see Figure 9). The sensitivity of normalized tropospheric ozone to fractional changes in methane and to fractional changes in the 150 hPa ozone flux is roughly similar, about 10-20% (Table 3). The sensitivity to the ozone flux is generally higher at 500 hPa than at the surface, with the largest sensitivity at the northernmost 500 hPa ozonesonde sites (0.24-0.25). The sensitivity to the methane is higher at the surface than at 500 hPa with the highest sensitivity at Arkona (0.45). The high sensitivity to methane at Arkona is likely due to the locally high NO_X emissions at the site. We also note that the regressed fit is poorest at Arkona. The sensitivity of the overall 30-90^o averaged ozone concentration is similar to the sensitivity at the various sites. The sensitivity coefficients will likely be somewhat sensitive to the tropospheric chemical mechanism, although the sensitivity may not be large for background chemical conditions.

As discussed above the non-linearity in the simulated long-term tropospheric ozone trend with respect to methane can be ascribed to the long-term modulation of the ozone flux at 150 hPa. However, the regression also captures many of the short-term changes in the simulated ozone (Figure 9). Since methane is only slowly changing, the short term ozone variability is due to variations in the flux of ozone across 150 hPa. Interestingly, the regressed fit does not capture the ensemble average ozone change during the Mt Pinatubo period. The portion of the simulated ozone record not explained by methane changes is obtained by subtracting the dependence of ozone on methane (determined from the regressed fit) from the simulated ozone record. In table 3 we give the correlation between this quantity and the vertical flux of ozone across 150 hPa averaged from 30-90^o N. The area-averaged correlations are large, ranging from 0.83 at 500 hPa to 0.74 at the surface.

At 500 hPa the correlation at individual sites is similar to the area-wide correlation except over Japan, although even over Japan the correlation is significant. At the surface the correlations at elevated sites are similar to the area-wide correlation. The variability explained by the stratospheric flux is low and not significant at Arkona, situated in a region of relatively large local emissions.. At Mace Head the stratospheric flux is only marginally correlated with the simulated record (Table 3). As shown below the Mace Head site is significantly impacted by European emissions. Sampling the simulations Northwest of Mace Head (by 10^o longitude west and by 5^o latitude north) significantly improves the correlation with the stratospheric ozone flux (Table 3). In the absence of daily output data from these simulations, it is likely that this displaced location will be more representative of the filtered baseline ozone measurements at Mace Head [*Simmonds et al.*, 2004; *Derwent et al.*, 2007] than sampling the model at the actual location of Mace Head. *Hess and Zbinden* [2013] found that the stratospherically tagged ozone has a large influence on the variability at the Mace Head site.

4.3 Response of tropospheric ozone to stratospheric ozone perturbations

The large-scale area-averaged simulated ozone variability is highly correlated across vertical levels (Figure 10) in all simulations. In this figure we subtract out the linear growth of tropospheric ozone due to methane changes. Stratospheric ozone is not detrended in this analysis so the impact of stratospheric ozone depletion and recovery on long timescales is retained. Detrended tropospheric ozone at the 500 and 1000 hPa levels is consistent with the long-term trends in stratospheric ozone: at all levels detrended tropospheric ozone is a maximum near 1970 and a minimum during the period influenced by the Mt Pinatubo eruption in the early 1990s. The shorter-term year-to-year fluctuations in ozone are also highly correlated in all simulations for each ensemble members. The correlation between the 150 hPa area averaged ozone and the detrended tropospheric area average at 500 hPa reaches 0.80 with a lag of 3 months; the correlation between 150 hPa and surface ozone reaches 0.75 with a lag of 4 months; the correlation between area-averaged 500 hPa ozone and the surface reaches 0.90 with a lag of 1 month. All these correlations are highly significant. *Hess and Zbinden* [2013] also discussed large-scale modeled and measured ozone correlations between the lower stratosphere and the surface, and found the correlations to be significant. On a more regional or local scale *Tarasick* [2005], *Ordóñez et al.* [2007], *Thouret et al.* [2006] and *Terao et al.* [2008] have reported significant measured correlations between stratospheric and tropospheric ozone. *Neu et al.* [2014] shows a vertical correlation in satellite retrieved ozone anomalies between 150 and 500 hPa and shows the correlation between stratospheric and tropospheric ozone is a good proxy for the relationship between tropospheric ozone and changes in STE. *Tang et al.* [2013] simulates the impact on tropospheric ozone of the large-scale stratospheric ozone reductions during the Mt Pinatubo period.

The overall response of 500 hPa ozone (averaged from 30-90^o N) to changes in 150 hPa ozone flux (averaged from 30-90^o N) is 0.018 ppb/ppb (not shown). Given a 150 ppb decrease in stratospheric ozone between approximately 1970 and the Mt Pinatubo period, the resulting ozone at 500 hP would have decreased by 2.7 ppb as a result. At individual stations the tropospheric response is stronger. The slope of surface ozone to stratospheric

perturbations is 0.007 ppb/ppb. This implies an area wide ozone decrease of approximately 1 ppb due to stratospheric ozone depletion. The overall response at the surface to ozone perturbations at 500 hPa is .38 ppb/ppb. As shown by *Hess and Zbinden* [2013], *Tang et al.* [2013] and *Zeng and Pyle* [2005] the tropospheric ozone response to increased STE is buffered by increases in tropospheric chemical ozone loss and deposition.

4.4 Coupled Modes of variability

The spatial pattern of ozone variability at 150 hPa, 500 hPa and the surface is analyzed using empirical orthogonal function (EOF) analysis. This analysis separates ozone variability into orthogonal basis functions. Each function is specified by a spatial pattern (with a dependence on location only) and a time-series for the temporal variations of this pattern with a dependence only on time (the principal component time series). EOF analysis allows an understanding of the geographic variability of the ozone record and relates the variability at different locations.

The EOF analysis is conducted on the detrended ozone record at all locations from 30-90^{o} N. The ozone record at the surface and 500 hPa are detrended by regressing ozone against global methane concentrations; the ozone record at 150 hPa is detrended with respect to time. The first EOF component at all three levels is given in Figure 11. The EOF is normalized so that its value gives the standard deviation of the ozone variations due to this EOF; the sign specifies the phase difference between the ozone variations explained by the EOF. Points with different sign have opposite temporal phases. The EOF captures from 40-48% of the ozone variability at the surface, 71-77% of the variability at 500 hPa and 79-85% of the variability at 150 hPa (Table 4).

For each ensemble member the correlation between the temporal variability of the principal component and the detrended area average ozone is very high (greater than 0.95 on all three levels, not shown). Thus, the temporal variation in EOFs is closely related to the area averaged ozone variations. However, the use of EOFs refines the simple use of area-averages by showing geographical differences in the pattern of variability with a better statistical characterization of the variability.

For each ensemble member, the principal component timeseries are highly correlated across vertical levels (Figure 12 and Table 4) suggesting the modes of variability isolated by the EOF analysis are physically deep. Due to the large ozone gradients between the stratosphere and troposphere, it is difficult to escape the conclusion that the coupled variability between the stratospheric and tropospheric levels is linked through the transport of high stratospheric ozone concentrations to the troposphere [see *Neu et al.*, 2014]. This is consistent with the analysis of *Hess and Zbinden* [2013]. As discussed below, the geographical pattern of the variability supports this conclusion.

The ensemble average of the area-averaged 30-90^{o} N ozone flux at 150 hPa explains 40% of the variability of the ensemble average of the principal component timeseries at the surface, 58% at 500 hPa and 69% at 150 hPa (with a lag of 3 to 9 months) (Table 4). The

691 lag increases as one descends in the atmosphere consistent with timescales for the
692 transport of ozone from the lowermost stratosphere to the surface. Individual correlations
693 between the ozone flux for each ensemble member and the principal component time
694 series for that ensemble member (instead of the correlation between the ensemble
695 averages) reduces the variability explained by the ozone flux to between approximately
696 10 and 23% (Table 4). Evidently the ensemble average of the respective timeseries
697 removes uncorrelated "noise" from each record. Analogous results also occur in an
698 analysis of the area-averaged ozone at each level (not shown).
699
700 The geographical pattern of the EOFs relates variability between different regions. On
701 each level the variability explained by this EOF is mostly the same sign (Figure 11)
702 consistent with the relationship between the principal component time series and that of
703 area averaged 30-90^{o} N ozone. At all levels the ozone variability attributed to the first
704 principal component is largest to the north and decreases to the south. The equatorward
705 decrease in the amplitude of the EOF is less at the surface, consistent with the transport
706 of stratospherically derived ozone downwards and southwards along isentropic surfaces.
707 The standard deviation of the ozone variation due to the first EOF reaches 0.6-0.8 ppb at
708 the surface, 1.5-2.0 ppb at 500 hPa and almost 80 ppb at 150 hPa. Obviously, at times the
709 amplitude of the first principal component can well exceed these values. At the end of
710 this section we examine the variation of the principal component at select measurement
711 locations.
712
713 *Hess and Zbinden* [2013] and *Zbinden et al.* [2006] noted the temporal variability of the
714 ozone record is often similar over widespread geographical regions. The large percent of
715 variability explained by the first EOF, the global nature of this mode, and the fact that it
716 is of the same sign over large regions of the N.H. extratropics demonstrates the
717 connection of the temporal ozone record between geographically distant regions. The
718 vertical coupling between the principal component timeseries of the first EOF and its
719 relation to the 150 hPa ozone flux suggests the root cause of this widespread variability is
720 due to coupled modes of stratosphere-troposphere variability. It seems likely the region
721 west of Ireland where the surface amplitude of the first EOF is large (Figure 11) is
722 captured by the measurements at the Mace Head observatory, particularly when the
723 measurements are sampled for "baseline" tropospheric air. This region of large amplitude
724 in the surface EOF pattern (Figure 11c) helps to explain the relation between the ozone
725 variability sampled at Mace Head and the variability sampled at the high alpine sites over
726 Europe [e.g., *Hess and Zbinden*, 2013], where the amplitude of the first EOF is also large.
727 The 150 hPa and 500 hPa ozonesondes over Canada, Northern Europe and Central
728 Europe also have similar amplitudes of the primary EOF. This suggests the variability
729 between these regions should be highly related as shown in *Hess and Zbinden* [2013].
730 The amplitude of this mode of variability is less over Japan at both 150 and 500 hPa: the
731 ozone variability over Japan is more likely to be swamped by other modes of variability.
732 As remarked above [also see *Hess and Zbinden*, 2013] the variability over Japan is not
733 well correlated with the variability in other regions.
734
735 At the surface (Figure 11c) the first EOF is small to occasionally negative over the
736 regions with high emissions: the Eastern U.S., Europe and Eastern Asia. In these regions

737 variability is likely governed by local photochemistry and is less influenced by the large-
738 scale processes examined here. In addition, since ozone has a different seasonality
739 between these locations and the more remote regions, annually averaged ozone is likely
740 to reflect different processes. Over the U.S. and Europe surface ozone tends to maximize
741 in summer; in other more remote locations ozone is minimum during the summer months.
742 Over Asia the seasonal variability is likely complicated by the summer monsoon. The
743 EOF pattern as a whole is dominated by variability over remote regions.
744
745 The geographic pattern of ozone variability associated with the first EOF reflects known
746 patterns of stratosphere-troposphere exchange (Figure 11) particularly at the surface. At
747 the surface high regions of variability extend southward over the Eastern Atlantic ocean
748 and the Eastern Pacific Ocean and the Western U.S. *Lin et al.* [2012], *James* [2003] and
749 *Sprenger* [2003] emphasizes the importance of deep stratospheric ozone intrusions over
750 the Western U.S. coast and Eastern Pacific. Here downward ozone transport from
751 stratospheric sources of ozone can descend along the Eastern flank of the Pacific
752 anticyclone. The outlines of this anti-cyclonic transport of ozone are particularly evident
753 at 1000 and 500 hPa in the first EOF (Figure 11). *Sprenger* [2003] also shows that the
754 Atlantic basin is a region of significant stratosphere to troposphere transport of air with a
755 climatological region of deep stratosphere to troposphere exchange extending from
756 southern Greenland to Ireland.
757
758 While the surface EOFs calculated for ensemble member are overall qualitatively similar,
759 rather large differences are notable in some locations between the different ensembles
760 (Figure S7). In particular, the Western U.S. and Ireland in particular show large
761 differences between different simulations, suggesting the importance of unforced model
762 variability in these regions. For example in one ensemble member ozone variability off
763 the Southwest Coast of the U.S. attributed to the first EOF exceeds 0.6 ppb, while in
764 another member it is less than approximately 0.2 ppb (Figure S7). The average variability
765 for all the ensembles is approximately 0.4 ppb (Figure 11). The magnitude of the first
766 EOF off Ireland also varies greatly between ensemble members: in one ensemble member
767 the variability attributed to the first EOF is approximately 0.7 ppb near Ireland, in another
768 ensemble member is close to zero with a mean close to 0.2 ppb (Figure 11).
769
770 The time series of the first principal component from each ensemble simulation show
771 little relation during some periods, but during others the ensembles show strong
772 similarities at all levels (Fig. 12). Many of the events where the ensembles show similar
773 behavior appear to be associated with ENSO (Figure 12): the pronounced negative and
774 positive ozone anomalies during all simulations and all levels during 1966 and 1967
775 appear to be associated with associated negative and positive ENSO indexes that occur 6-
776 12 months earlier; an ozone peak is also common to all levels and all ensembles in1998-
777 1999 following the El Nino of 1998. The 1998 El Nino event and a 1998-1999
778 tropospheric ozone anomaly has been linked in the literature [*Koumoutsaris et al.*, 2008;
779 *Voulgarakis et al.*, 2011]. However, we find the correlation between ENSO and the
780 principal component timeseries is small at all levels (less than 0.23) (not shown). (The
781 correlation is also small on all levels between the ENSO signal and the area averaged 30-
782 90^{o} ozone). We note that *Hsu and Prather* [2009] also did not find a relation between

ENSO and STE. However, *Zeng and Pyle* [2005] show a strong correlation between ENSO and stratosphere-troposphere exchange. Indeed the impact of ENSO on stratospheric circulation statistics via associated changes in stratospheric wave driving, and in particular an increase in the downwards residual velocity at extratropical latitudes during warm ENSO events, provides a mechanism whereby ENSO impacts the stratospheric-tropospheric exchange of ozone [*Calvo et al.*, 2010]. However, a careful examination of the ozone perturbations based on a compilation of high-index El Nino in *Calvo et al.* [2010] indicates significant ozone perturbations do not persist below about 10 km. In *Zeng and Pyle* [2005] the ENSO index and STE were only correlated between 1990-2002, a relatively short period compared to the present study. The simulations described in *Zeng and Pyle* [2005] did not include the forcing due the QBO or volcanoes included in the present study, forcings that may mask an underlying ENSO signal. *Neu et al.* [2014] were not able to isolate the impact of ENSO from that of the Quasi-Biennial Oscillation (QBO) on extratropical tropospheric ozone for the period from 2005 to 2011. The particular period examined in *Zeng and Pyle* [2005] (1990-2002) was also dominated by large events: the1998-1999 positive ozone anomaly associated with El Nino [*Koumoutsaris et al.*, 2008; *Voulgarakis et al.*, 2011] and the negative anomaly in 2000-2001 that can be associated with La Nina. Figure 12 suggests that only upon occasion does ENSO appear to be associated with the strong forcing of ozone anomalies, although, over the long-run the correlation between the two is small.

Sampled at characteristic locations (500 hPa Canadian sites, Mace Head, Lassen and the European alpine sites) (Figure 13) it is apparent that the ozone variability due to principal component timeseries explains a substantial fraction of the overall simulated variability. Over the course of the simulation the correlation between ozone variability and the principal component timeseries is: 0.97 for all ensemble simulations over the Canadian 500 hPa ozonesonde sites; between 0.64-0.80 for the ensemble simulations over the European alpine sites; between 0.48 and 0.70 for the ensemble simulations at Mace Head and between 0.09 and 0.74 for the ensemble simulations at Lassen. Note however at Lassen three of the simulations have correlations above 0.60. To better sample baseline ozone conditions at Mace Head we have sampled the model at the point 10^{o} West and 5^{o} North of the actual observatory location in Figure 13. The correlation between the model and measurements has been described above (section 3; also see Table 2)

Note in particular, the ozone increase between the measured ozone minimum in the early1990s and the ozone maximum near 1998-1999 at the disparate locations shown in Figure 13 is not only captured in the simulated ozone record but also in the principal component timeseries. At the four sites in Figure 13, the ozone jump during the 1990s (defined here as the maximum minus minimum annually averaged ozone during the 1990s, where the ozone has not been detrended) is 6.6 ppb at Mace Head, 7.4 ppb at the European Alpine, 9.1 ppb at Lassen and 12.6 ppb at the Canadian ozonesonde stations. The simulations capture approximately 50% of the measured increase at all stations, ranging from 47% over the Canadian stations to 56% at Mace Head. A regression against methane over entire the model simulation show that increases in methane explain a relatively small fraction of the ozone increase during the 1990s at these sites: 0.8 ppb/decade at the Lassen site, 0.27 ppb/decade over Canada, .39 ppb/decade at Mace

Head and 0.27 ppb/decade at the European Alpine sites. In fact, much of the simulated ozone increase at these sites can be traced to the principal component time series at these sites. Over Canada, the European Alpine sites, Lassen and Mace Head changes in the principal component account for 100%, 68%, 49% and 43% of the simulated ozone jump, showing that much of the jump during this period can be traced to changes in this global mode of variability. As argued above, the vertical correlation of the ozone principal component timeseries from the surface through the lower stratosphere, as well as their correlation with the 150 hPa ozone flux suggests changes in the principal component are consistent with changes in the STE of ozone. *Hess and Zbinden* [2013] show that much of the measured change ozone during the 1990s at a variety of tropospheric sites could be traced to increases in the stratospheric portion of ozone.

Ozone increases measured on the west coast of the U.S. at a variety of stations have been ascribed to increasing Asian emissions (e.g., [*Cooper et al.*, 2010]). However, the results here show substantial ozone increases have occurred during the 1990s over a wide variety of sites, many of them substantially removed from Asian emissions. In addition, the simulations, with no change in emissions, capture almost 50% of the observed ozone jump during the 1990s, including the changes at Lassen. This suggests that a large portion of the measured jump is not due to changes in emissions, but can be traced to changes in a global mode of ozone variability. This emphasizes the difficulty in the attribution of ozone changes, but also the importance of understanding the importance of natural variability in isolating the role of emissions in modifying ozone concentrations.

5. Conclusions

We have analyzed four ensemble free running simulations from 1953-2005 using the Whole Atmosphere Community Climate Model (WACCM). The simulations are forced by time changes in observed sea-surface temperatures, concentrations of greenhouse gases (including methane), stratospheric ozone depleting species, an externally forced quasi-biennial oscillation, solar variability and stratospheric sulfate surface area density (SAD). In the stratosphere WACCM employs a sophisticated chemical mechanism. In the troposphere only the basic tropospheric NO_X-CH_4 chemistry is used, where the NO_X surface emissions remain interannually constant. The relation between tropospheric interannual ozone variability and lower stratospheric interannual ozone variability is analyzed from 30-90^o N.

Despite the simplicity of the tropospheric chemistry, the simulations capture the measured N.H. background ozone interannual variability to a surprising extent. Particularly for the period after 1990 the simulated detrended ozone is significantly correlated with the measurements for the 500 hPa ozonesonde sites over Northern Europe, Central Europe and Canada (but not over Japan) and over surface measurement sites at Mace Head and the alpine sites over Europe (but not at Lassen or Arkona). We argue that the Arkona site (in Germany) is influenced by fresh anthropogenic emissions with a variability that may not be accurately captured with the simple tropospheric chemistry in these simulations. While the simulation appears to capture some aspects of the Lassen record, the large ozone trend in the measurements makes a simple comparison

875 difficult. Prior to 1990 there are fewer measurements and the reliability of the
876 measurements decreases. However, even during this period the simulated ozone record is
877 significantly correlated with the measured record in a number of locations.
878
879 It is not a foregone conclusion that the simulated detrended ozone should be correlated
880 with the measurements in the first place, as the model dynamics are internally calculated.
881 The fact that the model and observations are significantly correlated implies the
882 importance of external forcing in determining the ozone variability. Indeed, the
883 interannual simulated ozone record shows periods when the ozone variability appears to
884 have little relation between the different model ensemble simulations. However, these
885 periods are punctuated by times when the variability between the ensembles show strong
886 agreement suggesting the importance of a common forcing mechanism. At the sites
887 examined the correlation between the correlation between the different detrended
888 ensemble members ranges from approximately 0.24-0.44 at the surface to 0.4–0.5 at 500
889 and 150 hPa. The decade of the 1990s, in fact, may be particularly impacted by external
890 forcing due to the influence of Mt Pinatubo during the early part of the decade and the
891 impact of the 1998 El Nino toward the end of the decade.
892
893 There appears to be some association between the punctuated periods when all
894 all ensembles show strong agreement and ENSO. However, we do not find that these
895 periods occur with all ENSOs, even if the ENSO is particularly strong. We find little
896 relation between the El Nino Southern Oscillation (ENSO) index and large-scale
897 tropospheric ozone variability over the long-term record. We argue the length of the
898 simulated record in the current study and the inclusion of volcanic and QBO forcing may
899 explain the difference between this study and earlier work [e.g., *Zeng and Pyle*, 2005].
900
901 The simulated curves of ozone versus methane at a number of sites show a relatively
902 rapid ozone increase prior to 1970-1980, a subsequent slow down in the rate of ozone
903 increase from 1955-1970, but subsequent increased ozone growth after approximately
904 1990. The measured curves are strongly impacted by changes in ozone precursor
905 emissions and thus despite some similarities with the simulations remain difficult to
906 interpret with respect to STE. The ensemble average tropospheric ozone record can
907 largely be explained as a linear combination of the 30-90^{o} area averaged 150 hPa ozone
908 flux and the global methane concentration. We use the former quantity as a proxy for
909 STE. The long-term non-linear rate of ozone increase with respect to methane can be
910 explained by changes in the downward ozone flux across the 150 hPa level. As expected
911 from the imposed change in greenhouse gas forcing, the strength of the residual
912 circulation increases throughout the simulations. This alone would act to increase the
913 downward extratropical N.H. stratospheric ozone flux with a resulting increase in
914 tropospheric ozone; however, stratospheric ozone depletion counteracts this. As a
915 consequence the 150 hPa ozone flux decreases between approximately 1970-1990 and
916 the rate of growth of tropospheric ozone with respect to methane slows. Subsequent to Mt
917 Pinatubo ozone increases in the extratropical N.H. stratosphere. This acts to increase the
918 150 hPa stratospheric ozone flux with resulting increases in tropospheric ozone. The
919 multivariate linear regression of ozone against methane and the 150 hPa ozone flux gives
920 an approximate 20% sensitivity (percent change in ozone to percent change in methane)

to changes in methane; the average sensitivity to the ozone flux is 19% at 500 hPa and 11% at the surface. Without ozone depletion the approximate 15% increase in the simulated residual circulation from 1952 -2005 would have resulted in a consequent 1.5% increase in surface ozone in the N.H. extrattropics. Ozone depletion has reduced these increases by approximately half. A 30% increase in the ozone flux by 2100 [*Hegglin and Shepherd*, 2009] would result in 3% increase in surface ozone and a 6% increase in 500 hPa ozone.

On an interannual timescale changes in the ensemble averaged 150 hPa ozone flux (averaged from 30-90^{o} N) explains 70% of the ensemble averaged extratropical detrended ozone variability at 500 hPa and 55% of the ensemble averaged ozone variability at the surface. In regions of large emissions (e.g., Arkona) the variability explained is much less. Sampling "baseline" air just to the Northwest of Mace Head suggests variations in the ozone flux explain almost 25% of the variability of the "baseline" tropospheric ozone variability at Mace Head.

The first empirical orthogonal function (EOF) of 30-90^{o} N ozone variability explains from 40% of the ozone variability at the surface to over 80% of the ozone variability at 150 hPa. The spatial pattern of this EOF at the surface is consistent with expected patterns of stratosphere-troposphere exchange, with a maximum off the west coast of the U.S. The EOF also shows appreciable amplitude off the west coast of Ireland. The EOF has a small amplitude over regions with significant emissions of ozone precursors. The principal component timeseries associated with the first EOF are highly correlated in the vertical. The ensemble average principal component time series is also highly correlated with the ensemble average 150 hPa ozone flux and is highly correlated with the ensemble averaged 30-90^{o} ozone average.

The interannual ozone variability at a number of individual sites over the course of the model simulation is largely explained by the variability in the principal component of the global EOF. At the stations examined in detail (the Canadian ozonesonde stations, the European Alpine sites, Lassen and Mace Head) the simulated ozone increase during the 1990s is about 50% of the measured increase. Over Canada, the European Alpine sites, Lassen and Mace Head changes in the principal component account for 100%, 68%, 49% and 43% of the simulated ozone jump, showing that much of the jump during this period can be traced to changes in a global mode of ozone variability. This suggests that a large portion of the ozone increase in the 1990s as measured at a number of sites is not due to changes in emissions, but can be traced to changes in a global mode of ozone variability. This emphases the difficulty in the attribution of ozone changes, and the importance of natural variability in understanding the trends and variability of ozone [see *Lin et al.*, 2014]. The mode of variability analyzed here shows strong stratosphere-troposphere coupling, demonstrating the importance of the stratosphere in an attribution of tropospheric ozone variability.

Despite the simplicity of the tropospheric chemistry used in these simulations, the simulations match the observed tropospheric variability to a large extent over locations sampling background tropospheric air. It is expected that the introduction of additional

hydrocarbon chemistry as well as episodic emission variability (e.g., biomass burning) will introduce modes of variability not captured here as well as possibly dampen the basic modes of ozone variability analyzed above. Future simulations are necessary to fully explicate the importance of episodic emission variability and of the variability associated with hydrocarbon chemistry including that of biogenic emissions. However, based on the agreement between these simulations and measurements we hypothesize that the base state modes of variability isolated here are fundamental to the coupled troposphere-stratosphere chemical system. The results obtained here are largely consistent with those in *Hess and Zbinden* [2013], where a sophisticated tropospheric mechanism is employed along with methodology for tagging stratospheric ozone. *Hess and Zbinden* [2013] also found the exchange of ozone from the stratosphere to the troposphere explains a large fraction of extratropical ozone variability, even at the surface, and this variability operates on hemispheric spatial scales.

The high variability explained by this global mode and the fact that it is of the same sign over large regions of the N.H. extratropics demonstrates the relationship of the temporal ozone record between geographically distant tropospheric regions. *Hess and Zbinden* [2013] and *Zbinden et al.* [2006] noted the temporal variability of the ozone record is often similar over widespread geographical regions. The vertical coupling between the principal component timeseries of the first EOF and its relation to the 150 hPa ozone flux suggests the root cause of this widespread variability is due to coupled modes of stratosphere-troposphere variability.

It is perhaps surprising that the stratosphere should be so important in explaining interannual ozone variability. While early work suggested that much of the tropospheric ozone distribution can be explained with a stratospheric ozone source and a surface sink [*Levy et al.*, 1985], for the past several decades, a newer paradigm emerged which de-emphasized the role of the stratosphere. It was recognized that tropospheric photochemical ozone production is almost a order of magnitude larger than the input from the stratosphere e.g., [*Stevenson et al.*, 2006]. However, the stratospheric source of ozone is widespread [*Liang et al.*, 2009] and the lifetime of ozone is relatively large in the upper and middle stratosphere, allowing ozone to be transported throughout the troposphere [*Liang et al.*, 2009]. By contrast, ozone production can be large near the surface, but this is more than compensated for by photochemical and surface ozone loss. The stratospheric source is particularly important in explaining the interannual variability of ozone away from regions of immediate photochemical production.

These results suggest the difficulty in the attribution of ozone changes without understanding the root causes of the natural variability of ozone. Simply examining changes in ozone precursor emissions, even on the decadal timescale, is insufficient to link changes in ozone to changes in emissions. A full attribution of ozone variability may require more sophisticated models with a good resolution of stratospheric processes.

Acknowledgement. P. G. Hess would like to acknowledge NSF grant #1042787 for supporting this work. Work at LLNL was performed under the auspices of the U.S. Department of Energy (DOE), Office of Science, Office of Biological and Environmental Research by Lawrence Livermore National Laboratory under contract DE-AC52-07NA27344 and supported by the Atmospheric Radiation Measurement Program of the Office of Science at the US Department of Energy. The CESM project is supported by the National Science foundation and the US Department of Energy. The National Center for Atmospheric Research is operated by the University Corporation for Atmospheric Research under sponsor ship of the National Science Foundation. We acknowledge the World Ozone and Ultraviolet Radiation Data Centre (WOUDC) for ozonesondes for providing the ozonesonde data, the U.S. National Park Service 2002 for providing Lassen NP ozone data and to D. Parrish for providing access to his surface ozone datasets.

1043

1044 References

1045 Andrews, D. G., J. R. Holton, and C. B. Leovy (1987), Middle atmosphere dynamics.,
1046 *Middle atmosphere dynamics*.. *D. G. Andrews, J. R. Holton, C. B. Leovy.Academic*
1047 *Press, New York, NY, USA. 489 pp.*

1048 Butchart, N., A. A. Scaife, M. Bourqui, J. de Grandpre, S. H. E. Hare, J. Kettleborough,
1049 U. Langematz, E. Manzini, F. Sassi, and K. Shibata (2006), Simulations of
1050 anthropogenic change in the strength of the Brewer–Dobson circulation, *Climate*
1051 *Dynamics*, *27*(7), 727–741, doi:10.1007/s00382-006-0162-4.

1052 Butchart, N. et al. (2010), Chemistry–Climate Model Simulations of Twenty-First
1053 Century Stratospheric Climate and Circulation Changes, *Journal of Climate*, *23*(20),
1054 5349–5374, doi:10.1175/2010JCLI3404.1.

1055 Calvo, N., R. R. Garcia, W. J. Randel, and D. R. Marsh (2010), Dynamical Mechanism
1056 for the Increase in Tropical Upwelling in the Lowermost Tropical Stratosphere
1057 during Warm ENSO Events, *Journal of the Atmospheric Sciences*, *67*(7), 2331–
1058 2340, doi:10.1175/2010JAS3433.1.

1059 Carslaw, D. C. (2005), On the changing seasonal cycles and trends of ozone at Mace
1060 Head, Ireland, *Atmospheric Chemistry and Physics Discussions*, *5*(4), 5987–6011.

1061 Cooper, O. R., D. D. Parrish, A. Stohl, M. Trainer, P. Nédélec, V. Thouret, J. P. Cammas,
1062 S. J. Oltmans, B. J. Johnson, and D. Tarasick (2010), Increasing springtime ozone
1063 mixing ratios in the free troposphere over western North America, *Nature*,
1064 *463*(7279), 344–348.

1065 Cui, J., S. Pandey Deolal, M. Sprenger, S. Henne, J. Staehelin, M. Steinbacher, and P.
1066 Nédélec (2011), Free tropospheric ozone changes over Europe as observed at
1067 Jungfraujoch (1990–2008): An analysis based on backward trajectories, *Journal of*
1068 *Geophysical Research*, *116*(D10), D10304, doi:10.1029/2010JD015154.

1069 Danielsen, E. F. (1968), Stratospheric-Tropospheric Exchange Based on Radioactivity,
1070 Ozone and Potential Vorticity, *Journal of the Atmospheric Sciences*, *25*(3), 502–518,
1071 doi:10.1175/1520-0469. (1968)025<0502:STEBOR>2.0.CO;2.

1072 Derwent, R. G., P. G. Simmonds, A. J. Manning, and T. G. Spain (2007), Trends over a
1073 20-year period from 1987 to 2007 in surface ozone at the atmospheric research
1074 station, Mace Head, Ireland, *Atmospheric Environment*, *41*(39), 9091–9098.

1075 Dlugokencky, E. J., E. G. Nisbet, R. Fisher, and D. Lowry (2011), Global atmospheric
1076 methane: budget, changes and dangers., *Philosophical transactions. Series A,*

1077 *Mathematical, physical, and engineering sciences*, *369*(1943), 2058–72,
1078 doi:10.1098/rsta.2010.0341.

1079 Eyring, V. et al. (2010a), Multi-model assessment of stratospheric ozone return dates and
1080 ozone recovery in CCMVal-2 models, *Atmospheric Chemistry and Physics*, *10*(19),
1081 9451–9472, doi:10.5194/acp-10-9451-2010.

1082 Eyring, V., T. G. Shepherd, and D. W. Waugh (2010b), Stratospheric Processes and their
1083 Role in Climate, WCRP - 132, WMO/TD - No. 1526, SPARC Report No. 5

1084 Gettleman, A., J. R. Holton, and H. Rosenlof (1997), Mass fluxes of O3, CH4, N2O and
1085 CF2CL2 in the lower stratosphere calculated from observational data, *Journal of*
1086 *Geophysical Research*, *102*(97), 19,149–19,159.

1087 Hegglin, M. I., and T. G. Shepherd (2009), Large climate-induced changes in ultraviolet
1088 index and stratosphere-to-troposphere ozone flux, *Nature Geoscience*, *2*, 687–691,
1089 doi:doi:10.1038/ngeo604.

1090 Hess, P. G., and J.-F. Lamarque (2007), Ozone source attribution and its modulation by
1091 the Arctic oscillation during the spring months, *Journal of Geophysical Research*,
1092 *112*(D11), 1–17, doi:10.1029/2006JD007557.

1093 Hess, P. G., and R. Zbinden (2013), Stratospheric impact on tropospheric ozone
1094 variability and trends: 1990–2009, *Atmospheric Chemistry and Physics*, *13*(2), 649–
1095 674, doi:10.5194/acp-13-649-2013.

1096 Hsu, J., and M. J. Prather (2009), Stratospheric variability and tropospheric ozone,
1097 *J.Geophys.Res.*, *114*(D6), D06102, doi:doi:10.1029/2008JD010942.

1098 Jaffe, D., D. Chand, W. Hafner, A. Westerling, and D. Spracklen (2008), Influence of
1099 Fires on O3 Concentrations in the Western US, *Environ. Sci. Technol.*, *42*, 5885–
1100 5891.

1101 James, P. (2003), A 15-year climatology of stratosphere–troposphere exchange with a
1102 Lagrangian particle dispersion model 2. Mean climate and seasonal variability,
1103 *Journal of Geophysical Research*, *108*(D12), 8522, doi:10.1029/2002JD002639.

1104 Konovalov, I. B., M. Beekmann, I. N. Kuznetsova, a. Yurova, and a. M. Zvyagintsev
1105 (2011), Atmospheric impacts of the 2010 Russian wildfires: integrating modelling
1106 and measurements of an extreme air pollution episode in the Moscow region,
1107 *Atmospheric Chemistry and Physics*, *11*(19), 10031–10056, doi:10.5194/acp-11-
1108 10031-2011.

1109 Koumoutsaris, S., I. Bey, S. Generoso, and V. Thouret (2008), Influence of El Niño–
1110 Southern Oscillation on the interannual variability of tropospheric ozone in the

1111 northern midlatitudes, *Journal of Geophysical Research*, *113*(D19), 1–21,
1112 doi:10.1029/2007JD009753.

1113 Lamarque, J.-F., and P. G. Hess (2003), Model analysis of the temporal and geographical
1114 origin of the CO distribution during the TOPSE campaign, *Journal of Geophysical*
1115 *Research.D.Atmospheres*, *108*(D4), doi:10.1029/2002JD002077.

1116 Lamarque, J.-F. et al. (2010), Historical (1850–2000) gridded anthropogenic and biomass
1117 burning emissions of reactive gases and aerosols: methodology and application,
1118 *Atmospheric Chemistry and Physics*, *10*(15), 7017–7039, doi:10.5194/acp-10-7017-
1119 2010.

1120 Lamarque, J.-F. et al. (2012), CAM-chem: description and evaluation of interactive
1121 atmospheric chemistry in the Community Earth System Model, *Geoscientific Model*
1122 *Development*, *5*(2), 369–411, doi:10.5194/gmd-5-369-2012.

1123 Leibensperger, E. M., L. J. Mickley, and D. J. Jacob (2008), Sensitivity of US air quality
1124 to mid-latitude cyclone frequency and implications of 1980-2006 climate change,
1125 *Atmospheric Chemistry and Physics*, *8*(23), 7075–7086.

1126 Levy, H., J. D. Mahlman, W. J. Moxim, and S. C. Liu (1985), Tropospheric ozone: The
1127 role of transport, *Journal of Geophysical Research*, *90*(D2), 3753,
1128 doi:10.1029/JD090iD02p03753.

1129 Liang, Q. et al. (2009), and Physics The governing processes and timescales of
1130 stratosphere-to-troposphere transport and its contribution to ozone in the Arctic
1131 troposphere, *Atmos. Chem. Phys.*, *9*, 3011–3025.

1132 Lin, M., A. M. Fiore, O. R. Cooper, L. W. Horowitz, A. O. Langford, H. Levy, B. J.
1133 Johnson, V. Naik, S. J. Oltmans, and C. J. Senff (2012), Springtime high surface
1134 ozone events over the western United States: Quantifying the role of stratospheric
1135 intrusions, *Journal of Geophysical Research: Atmospheres*, *117*(D21),
1136 doi:10.1029/2012JD018151.

1137 Lin, M., L. W. Horowitz, S. J. Oltmans, A. M. Fiore, and S. Fan (2014), Tropospheric
1138 ozone trends at Mauna Loa Observatory tied to decadal climate variability,
1139 doi:10.1038/NGEO2066.

1140 Logan, J. A. et al. (2012), Changes in ozone over Europe: Analysis of ozone
1141 measurements from sondes, regular aircraft (MOZAIC) and alpine surface sites,
1142 *Journal of Geophysical Research*, *117*(D9), D09301, doi:10.1029/2011JD016952.

1143 Marenco, A., H. Gouget, P. Nédélec, J.-P. Pagés, and F. Karcher (1994), Evidence of a
1144 long-term increase in tropospheric ozone from Pic du Midi data series:
1145 Consequences: Positive radiative forcing, *J.Geophys.Res.*, *99*(D8), 16617–16632.

1146 Neu, J. L., T. Flury, G. L. Manney, M. L. Santee, N. J. Livesey, and J. Worden (2014),
1147 Tropospheric ozone variations governed by changes in stratospheric circulation,
1148 340–344, doi:10.1038/NGEO2138.

1149 Office of Air Quality Planning and Standards, U. E., National Air Pollutant Emission
1150 Trends: 1900-1998.

1151 Ohara, T., H. Akimoto, J. Kurokawa, N. Horii, K. Yamaji, X. Yan, and T. Hayasaka
1152 (2007), An Asian emission inventory of anthropogenic emission sources for the
1153 period 1980–2020, *Atmospheric Chemistry and Physics*, *7*(16), 4419–4444,
1154 doi:10.5194/acp-7-4419-2007.

1155 Oltmans, S. J., B. J. Johnson, and J. M. Harris (2012), Springtime boundary layer ozone
1156 depletion at Barrow, Alaska: Meteorological influence, year-to-year variation, and
1157 long-term change, *Journal of Geophysical Research*, *117*, D00R18,
1158 doi:10.1029/2011JD016889.

1159 Oman, L. D. et al. (2010), Multimodel assessment of the factors driving stratospheric
1160 ozone evolution over the 21st century, *Journal of Geophysical Research*, *115*(D24),
1161 D24306, doi:10.1029/2010JD014362.

1162 Ordóñez, C., D. Brunner, J. Staehelin, P. Hadjinicolaou, J. a. Pyle, M. Jonas, H. Wernli,
1163 and a. S. H. Prévôt (2007), Strong influence of lowermost stratospheric ozone on
1164 lower tropospheric background ozone changes over Europe, *Geophysical Research*
1165 *Letters*, *34*(7), 1–5, doi:10.1029/2006GL029113.

1166 Parrish, D. D. et al. (2012), Long-term changes in lower tropospheric baseline ozone
1167 concentrations at northern mid-latitudes, *Atmospheric Chemistry and Physics*,
1168 *12*(23), 11485–11504, doi:10.5194/acp-12-11485-2012.

1169 Parrish, D. D. et al. (2014), Long-term changes in lower tropospheric baseline ozone
1170 concentrations: Comparing chemistry-climate models and observations at northern
1171 midlatitudes, , (119), 5719–5736, doi:10.1002/2013JD021435.

1172 Pozzoli, L. (2011), Re-analysis of tropospheric sulfate aerosol and ozone for the period
1173 1980–2005 using the aerosol-chemistry-climate model ECHAM5-HAMMOZ,
1174 *Atmos. Chem. Phys., 11,* 9563-9594, doi:10.5194/acp-11-9563-2011.

1175 Simmonds, P. G., R. G. Derwent, A. L. Manning, and G. Spain (2004), Significant
1176 growth in surface ozone at Mace Head, Ireland, 1987-2003, *Atmospheric*
1177 *Environment*, *38*(28), 4769–4778, doi:10.1016/j.atmosenv.2004.04.036.

1178 Sprenger, M. (2003), A northern hemispheric climatology of cross-tropopause exchange
1179 for the ERA15 time period (1979–1993), *Journal of Geophysical Research*,
1180 *108*(D12), 8521, doi:10.1029/2002JD002636.

1181 Stevenson, D. S. et al. (2006), Multimodel ensemble simulations of present-day and near-
1182 future tropospheric ozone, *Journal of Geophysical Research*, *111*(D8),
1183 doi:10.1029/2005JD006338.

1184 Tang, Q., P. G. Hess, B. Brown-steiner, D. E. Kinnison, and E. Douglas (2013),
1185 Tropospheric ozone decrease due to the Mount Pinatubo eruption : Reduced
1186 stratospheric influx, *Geophysical Research Letters*, *40*(20), 5553–5558,
1187 doi:10.1002/2013GL056563.

1188 Tarasick, D. W. (2005), Changes in the vertical distribution of ozone over Canada from
1189 ozonesondes: 1980–2001, *Journal of Geophysical Research*, *110*(D2),
1190 doi:10.1029/2004JD004643.

1191 Terao, Y., J. a. Logan, A. R. Douglass, and R. S. Stolarski (2008), Contribution of
1192 stratospheric ozone to the interannual variability of tropospheric ozone in the
1193 northern extratropics, *Journal of Geophysical Research*, *113*(D18), 1–9,
1194 doi:10.1029/2008JD009854.

1195 Thouret, V., J. P. Cammas, B. Sauvage, G. Athier, R. Zbinden, P. Nédélec, P. Simon, and
1196 F. Karcher (2006), Tropopause referenced ozone climatology and inter-annual
1197 variability (1994–2003) from the MOZAIC programme, *Atmos. Chem. Phys*, *6*(4),
1198 1033–1051, doi:10.5194/acp-6-1033-2006.

1199 Tressol, M. et al. (2008), Air pollution during the 2003 European heat wave as seen by
1200 MOZAIC airliners, *Atmospheric Chemistry and Physics*, *8*(8), 2133–2150,
1201 doi:10.5194/acp-8-2133-2008.

1202 Turner, a. J., a. M. Fiore, L. W. Horowitz, and M. Bauer (2013), Summertime cyclones
1203 over the Great Lakes Storm Track from 1860–2100: variability, trends, and
1204 association with ozone pollution, *Atmospheric Chemistry and Physics*, *13*(2), 565–
1205 578, doi:10.5194/acp-13-565-2013.

1206 Vestreng, V., L. Ntziachristos, A. Semb, S. Reis, I. S. A. Isaksen, and L. Tarras (2009),
1207 Evolution of NOx emissions in Europe with focus on road transport control
1208 measures, *Atmospheric Chemstry and Physics,* 9(4), 1503–1520, doi:10.5194/acp-9-
1209 1503-2009.

1210 Volz, A., and D. Kley (1988), Evaluation of the Montsouris series of ozone
1211 measurements made in the nineteenth century, *Nature*, 240–242,
1212 doi:10.1038/332240a0.

1213 Voulgarakis, A., P. Hadjinicolaou, and J. A. Pyle (2011), Increases in global tropospheric
1214 ozone following an El Niño event: examining stratospheric ozone variability as a
1215 potential driver, *Atmospheric Science Letters*, *12*, 228–232, doi: 10.1002/asl.318.

Wilson, R. C., Z. L. Fleming, P. S. Monks, G. Clain, S. Henne, I. B. Konovalov, S. Szopa, and L. Menut (2012), Have primary emission reduction measures reduced ozone across Europe? An analysis of European rural background ozone trends 1996–2005, *Atmospheric Chemistry and Physics*, *12*(1), 437–454, doi:10.5194/acp-12-437-2012.

Zbinden, R. M., J. P. Cammas, V. Thouret, P. Nedelec, F. Karcher, and P. Simon (2006b), Mid-latitude tropospheric ozone columns from the MOZAIC program: climatology and interannual variability Atmos, *Chem.Phys*, *6*, 1053–1073.

Zeng, G., and J. A. Pyle (2005), Influence of El Nino Southern Oscillation on stratosphere/troposphere exchange and the global tropospheric ozone budget, *Geophysical Research Letters*, *32*(1), L01814.

Table 1: Measurement sites used in this paper.

Measurement Sites	Platform	Lon.	Lat.	Elev.
Canada				
Alert[1]	Ozonesonde	62° W	82° N	NA
Churchill[1]	Ozonesonde	94° W	59° N	NA
Eureka[1]	Ozonesonde	85° W	80° N	NA
Goose Bay[1]	Ozonesonde	60° W	53° N	NA
Resolute[1]	Ozonesonde	95° W	75° N	NA
Central Europe				
Debilt[2]	Ozonesonde	5° E	52° N	NA
Hohenpeissenberg[2]	Ozonesonde	11° E	48° N	NA
Leginowo[2]	Ozonesonde	21° E	52° N	NA
Lindenberg[2]	Ozonesonde	14° E	52° N	NA
Payerne[2]	Ozonesonde	8° E	47° N	NA
Uccle[2]	Ozonesonde	4° E	51° N	NA
Arkona[2]	Surface	13° E	54° N	42 m
Jungfraujoch[3]	Surface	8.0° E	47° N	3580m
Mace Head	Surface	10° W	53° N	25m
Zugspitze[3]	Surface	11° E	47° N	2960 m
Japan				
Kagoshima[4]	Ozonesonde	131°E	32°N	NA
Sapporo[4]	Ozonesonde	141°E	43°N	NA
Tateno[4]	Ozonesonde	140°E	36°N	NA
Northern Europe				
Ny Alesund[5]	Ozonesonde	12° E	79° N	NA
Scoresbysund[5]	Ozonesonde	22° W	70° N	NA
Sodankyla[5]	Ozonesonde	26° W	67° N	NA
United States				
Lassen	Surface	122° W	41° N	1769m

[1]Canadian ozonesonde sites averaged together [2]Central European ozonesonde sites averaged together [3]Central European alpine sites averaged together [4]Japanese ozonesonde sites are averaged together [5]Northern European ozonesonde sites are averaged together.

Table 2: Comparison between ensemble mean simulated and measured ozone at various sites.

STATIONS	YEARS[1]	MEAS MEAN (ppbv)	MODEL BIAS (ppbv)	CORRELATION[2] < 1990	CORRELATION[2] > 1990	ENSEMBLE[3] CORRELATION
150 hPa						
Canada	19660515- 20050915	627.1	13.6	**0.46**	**0.54**	0.22,**0.46**,0.52
N. Europe	19881215-20050915	602.9	6.9	--	0.57	0.21,**0.42**,0.53
C. Europe	19670215-20050915	423.9	11.2	**0.64**	0.32	0.14,**0.43**,0.55
Japan	19690515-20050915	242.4	-1.1	0.12	0.03	0.31,**0.40**,0.45
500 hPa						
Canada	19660515- 20050915	54.6	-2.1	**0.40**	**0.57**	0.29,**0.50**,0.57
N. Europe	19881215-20050915	57.9	-5.9	--	**0.73**	0.26,**0.47**, 0.56
C. Europe	19670215-20050915	60.0	-6.1	0.16	**0.66**	0.25,**0.49**,0.62
Japan	19690515-20050915	58.0	-4.2	-0.07	0.07	0.34,**0.42**,0.56
Surface						
JFJ/ZUG	19781015-20050915	50.9	-2.4	-0.16	**0.66**	0.24,**0.44**, 0.63
Lassen	19880915- 20050915	40.4	5.2	--	0.25	0.21,**0.31**,0.44
Macehead	19880115-20050915	38.5	-6.1	--	**0.65**	0.09,**0.39**,0.54
Arkona	19570515-20021115	28.7	-3.0	**0.63**	0.01	0.02,**0.25**,0.45

[1]Years over which measurements and the simulation are evaluated. [2]Correlation between 12-month smoothed detrended ensemble mean ozone and 12-month smoothed detrended measurements before and after 1990. Significant correlations (at 99%) are in bold. [3]Correlation between ensemble members: lowest correlation, median correlation, high correlation. Median correlations significant at 95% in bold. Correlations are between 12-month smoothed records. The bias is evaluated between 1990 and 2005.

Table 3: Sensitivity coefficients for the temporal regression for 12-month smoothed normalized simulated ozone with normalized globally averaged methane and the normalized lagged ozone flux. Coefficients given for the lag given the smallest chi squared.

Stations	SENSITIVITY CH4	SENSITIVITY FLUX	LAG[1] (months)	CORR[2]	CHISQ
500 hPa					
Canada	0.15	0.25	5	**0.86**	0.071
N Europe	0.16	0.24	6	**0.83**	0.088
C Europe	0.18	0.17	5	**0.77**	0.072
Japan	0.22	0.08	5	**0.47**	0.084
30-90 N Aver	0.17	0.19	4	**0.84**	0.053
Surface					
JFJ/ZUG	0.20	0.13	6	**0.67**	0.068
Lassen	0.15	0.14	5	**0.67**	0.082
Arkona	0.45	0.04	5 [3]	0.11	0.581
Mace Head	0.20	0.09	5	**0.28** [4]	0.307
30-90 N Aver	0.21	0.11	6	**0.73**	0.035

[1]Lag in months between the ozone record and the 30-90° N averaged ozone flux resulting in the smallest regressed chi-squared. The lag is measured as the number of months by which the ozone flux lags the ozone concentration. [2]Correlation is between the regressed ozone record and the simulated ozone record after removing the regressed dependence on methane from each (see text). Values significant at the 99% level are shown in bold. [3]There is no well defined minimum chi-squared at Arkona. We give coefficients at five months. [4] Correlation is 0.49 for the point 10° West and 5° North of Mace Head.

Table 4. Explained variances and correlations between EOFs on various model levels.

LEVEL	Explained Variance[1]	Correlation 150 hPa PC[2]	Correlation O3 FLUX 150 hPa[3]	Lag[4]
150 hPa	79-85%	NA	0.83 (0.46)	3 (3)
500 hPa	71-77%	0.78	0.76 (0.48)	6 (6)
1000 hPa	40-48%	0.66	0.63 (0.32)	9 (9)

[1]Range of variances explained by the 1st EOF over the model ensembles [2]Temporal correlation between principal components at 1000 hPa and 500 hPa and the principal component at 150 hPa. Correlation is computed between levels of the same ensemble simulation; however, the overall correlation coefficient comprises the relationship for all ensembles. All correlations are significant at the 99% level. [3]Temporal lagged correlation between principal components on various pressure levels and the 30-90° N averaged ozone flux at 150 hPa. Without parenthesis: correlation between the ensemble averaged principal component and the ensemble averaged ozone flux; with parenthesis: correlation is computed between levels of the same ensemble simulation; however, the overall correlation coefficient comprises the relationship for all ensembles. All correlations are significant at the 99% level. [4]Lag (months) of the maximum correlation between the ozone flux and the principal component: without parenthesis for the ensemble average; with parenthesis for individual ensemble members. The lag is measured as the number of months by which the ozone flux lags the ozone concentration.

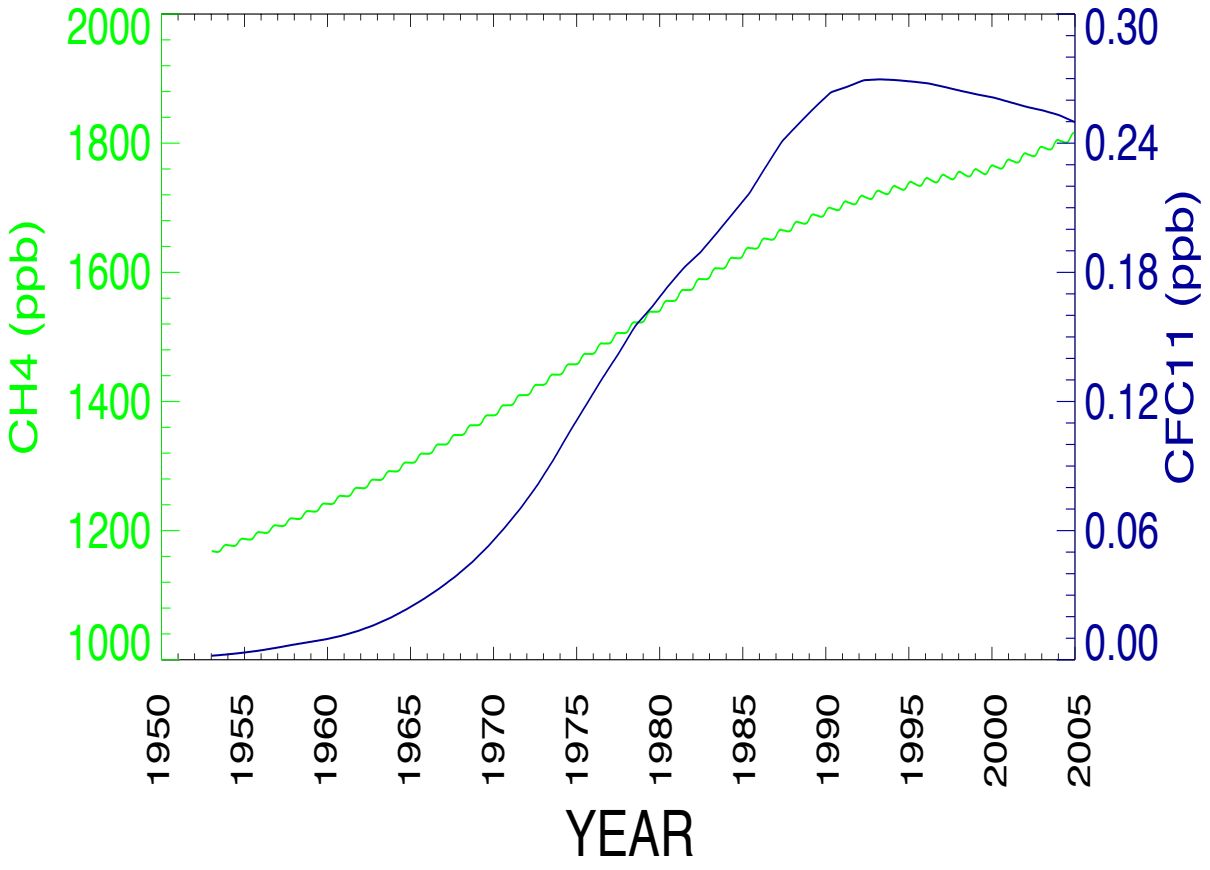

Figure 1: Model Forcings. Concentrations of CH_4 (green, left axis) and CFC-11 (blue, right axis) globally area-averaged at lower boundary and used to force the WACCM simulations.

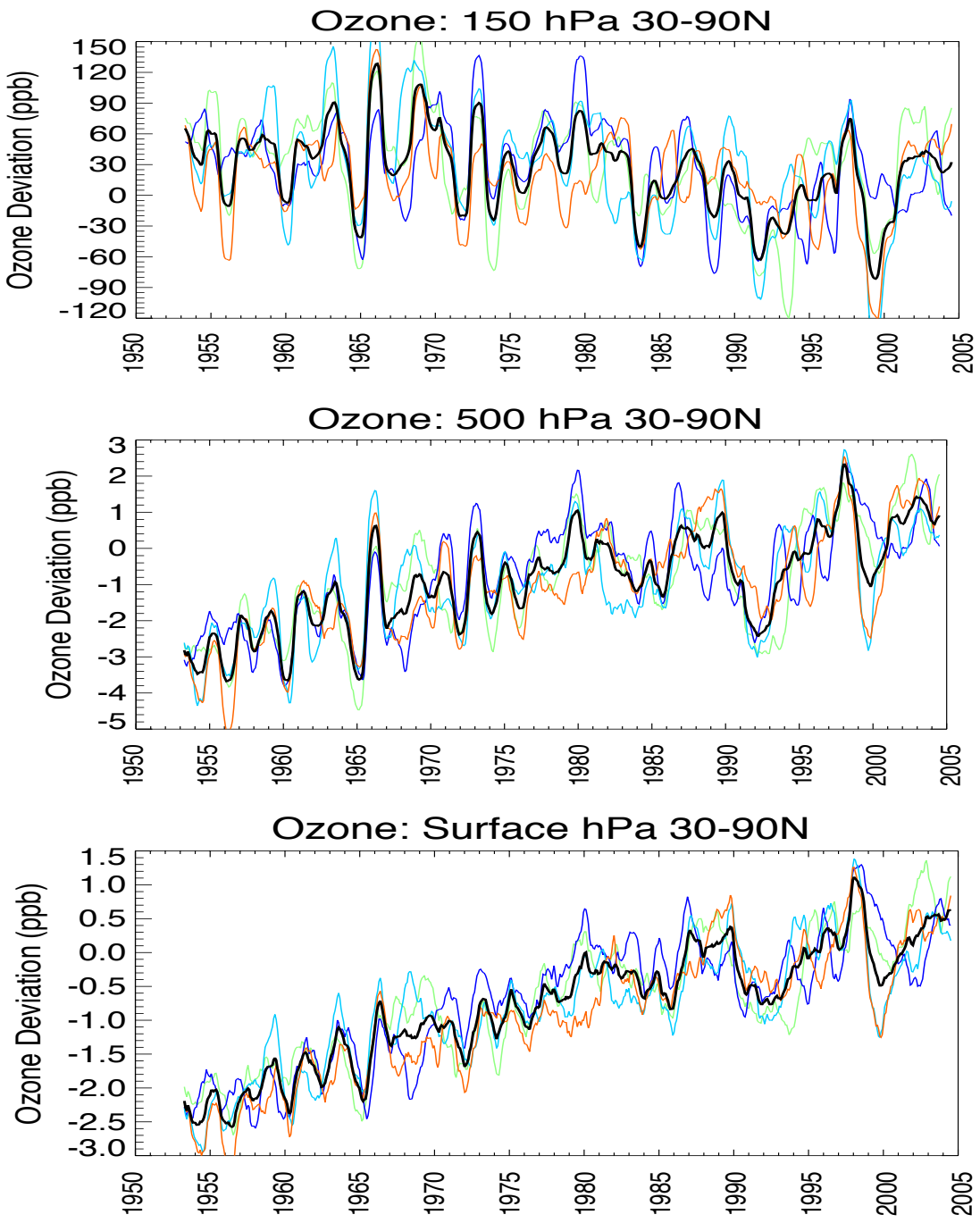

Figure 2: Ozone deviations (ppb) averaged from 30-90^{o} N for each WACCM ensemble member (colored) and the deviation averaged over all ensemble members (black). Monthly ozone deviations are smoothed over 12-months. Deviations are from ozone averaged 1990-01-15—1994-12-15.

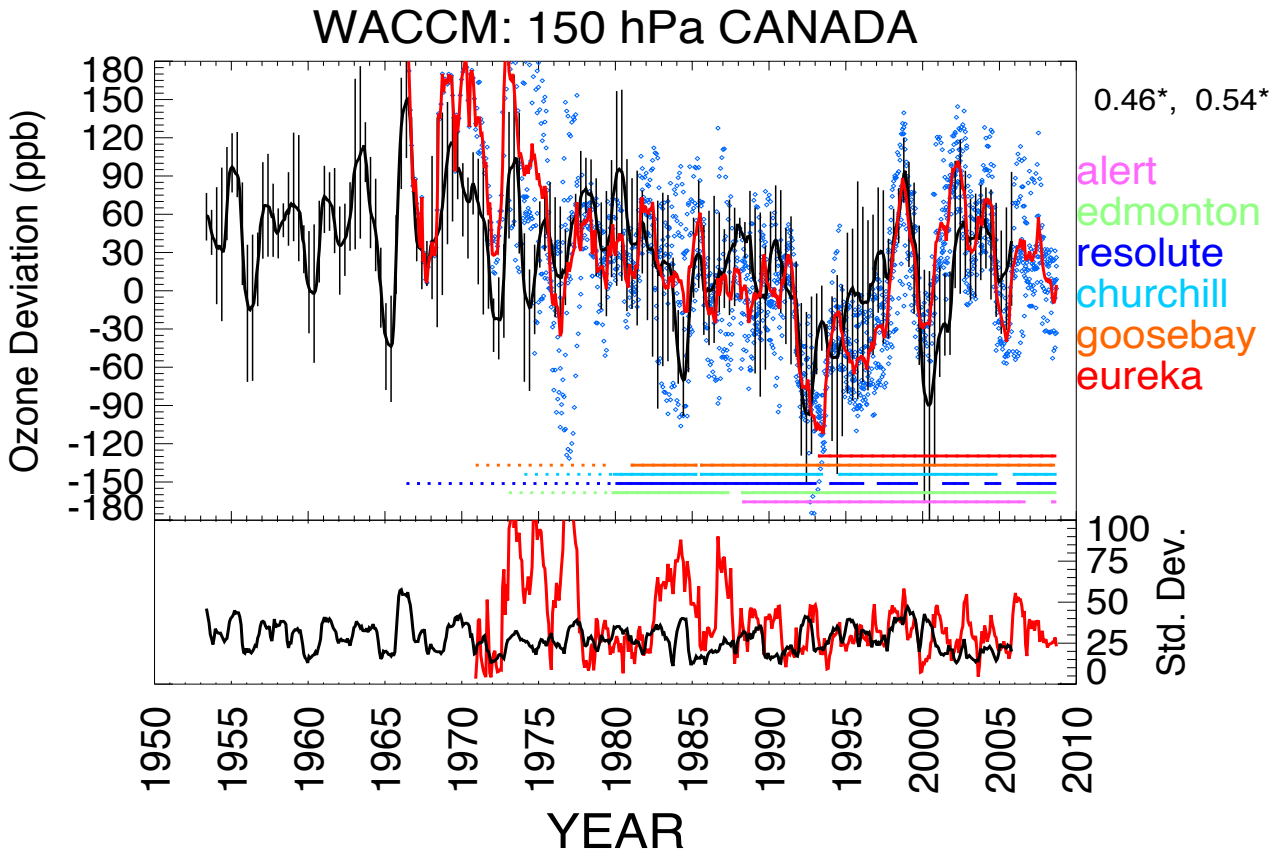

Fig. 3: Simulated and measured ozone deviations (ppb) averaged over the Canadian ozonesonde sites at 150 hPa. The simulated ensemble average is given as the bold black line, the thin black lines bracket the maximum and minimum ensemble ozone deviation, the measured average is given as the red line, the blue dots give the measured ozone deviation for each site comprising the regional average. Colored bars indicate when each measurement site (color coded as indicated on right) made sufficient measurements to calculate an annual ozone concentration: solid lines indicate an ECC measurement and dotted lines a BrewerMast ozonesonde measurement. The black and red lines at the bottom give the simulated (black) and measured (red) standard deviation of ozone (ppb) calculated across all sites within each region. Numbers in the upper right give the model-measurement correlation of the average ozone within each region prior to 1990 (left) and after 1990 (right). Correlations use detrended data. Significant correlations at the 95% level are starred. Monthly ozone deviations are smoothed over 12-months. Deviations are from ozone averaged 1990-01-15—1994-12-15.

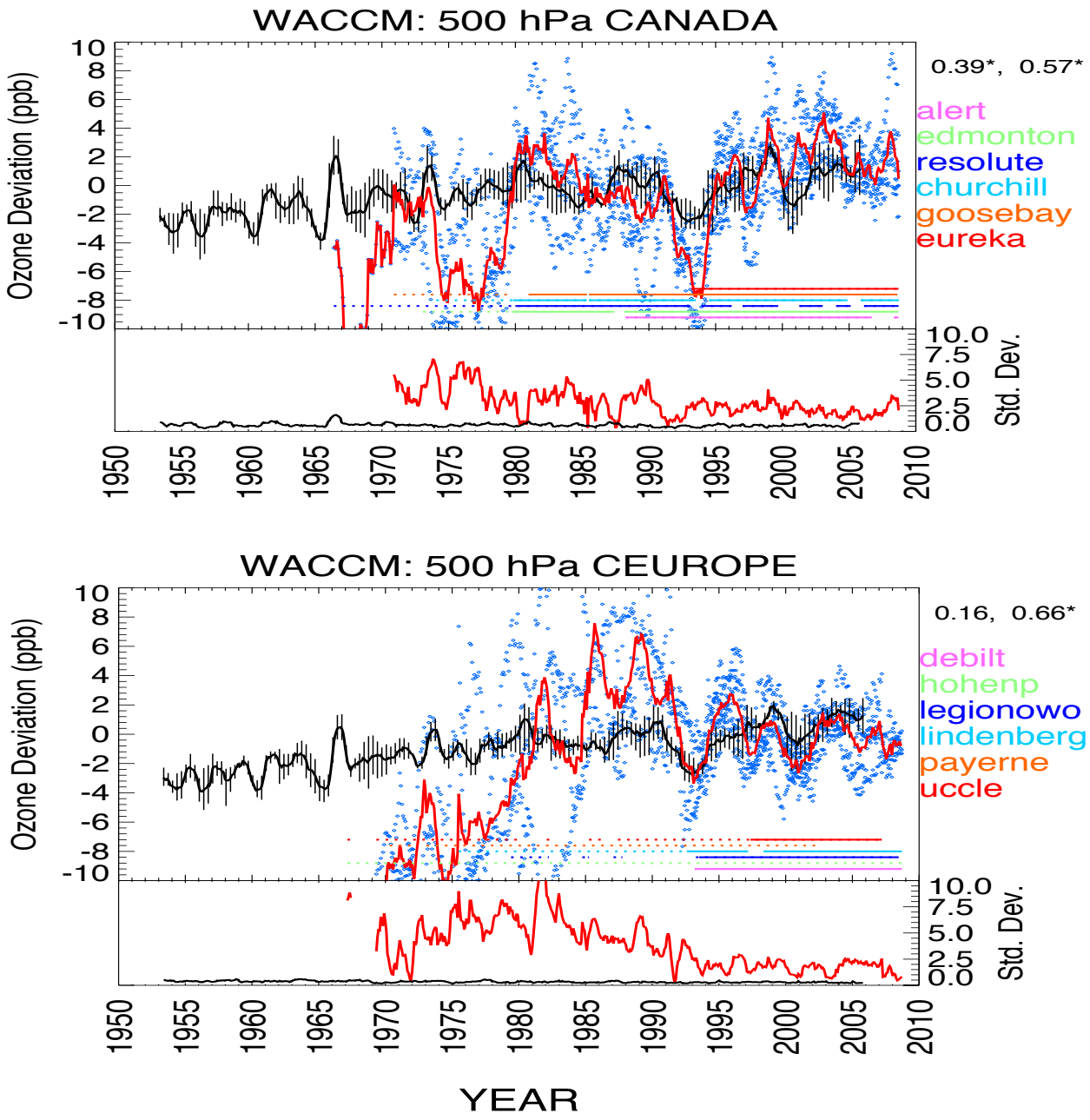

Fig. 4: As in Figure 3, but for the 500 hPa Canadian and Central European ozonesonde sites.

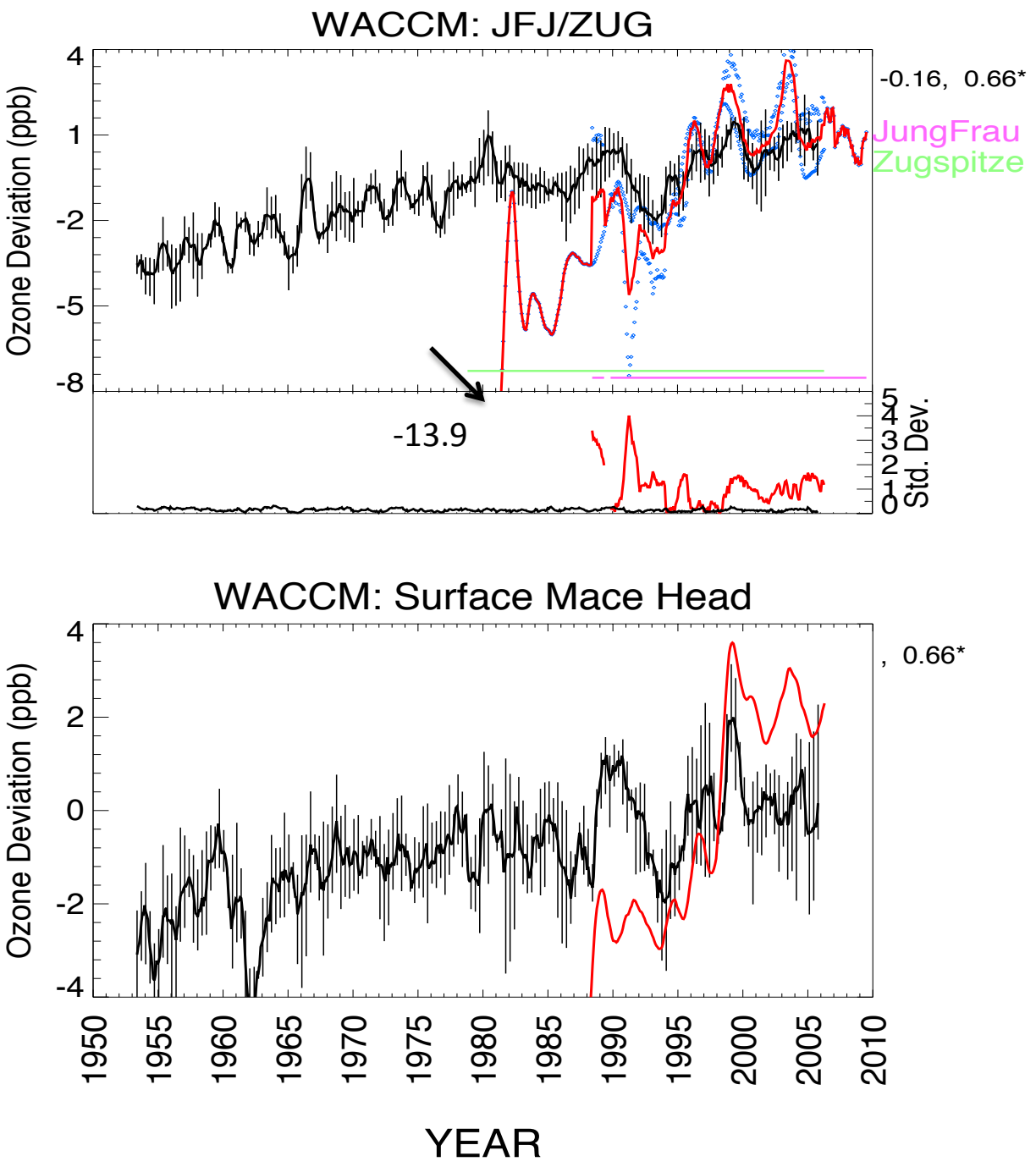

Fig. 5: As in Figure 3 but for the surface simulated and measured surface ozone deviations (ppb): a) averaged for the Jungfraujoch and Zugspitze sites; b) at Mace Head, Ireland. The bottom bars in (a) indicate the years for which an annually averaged measurement was available at the Jungfraujoch and Zugspitze sites.

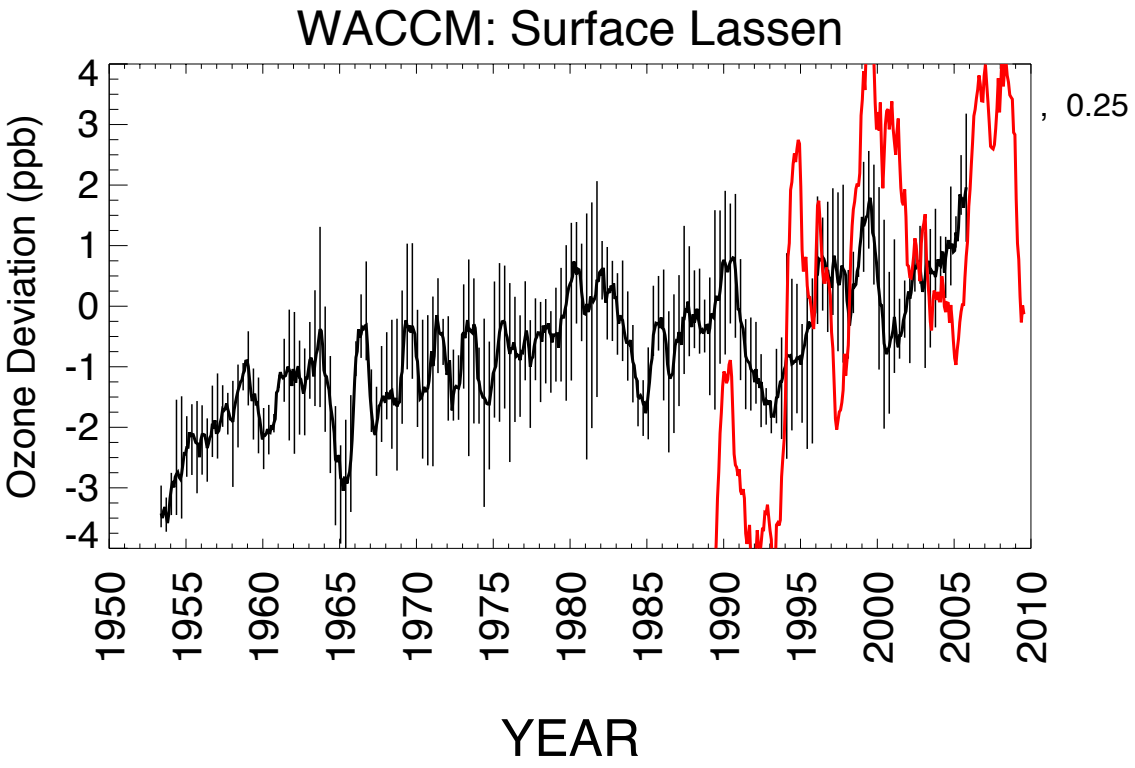

Fig. 6: As in Figure 5, but for surface measurements at Lassen.

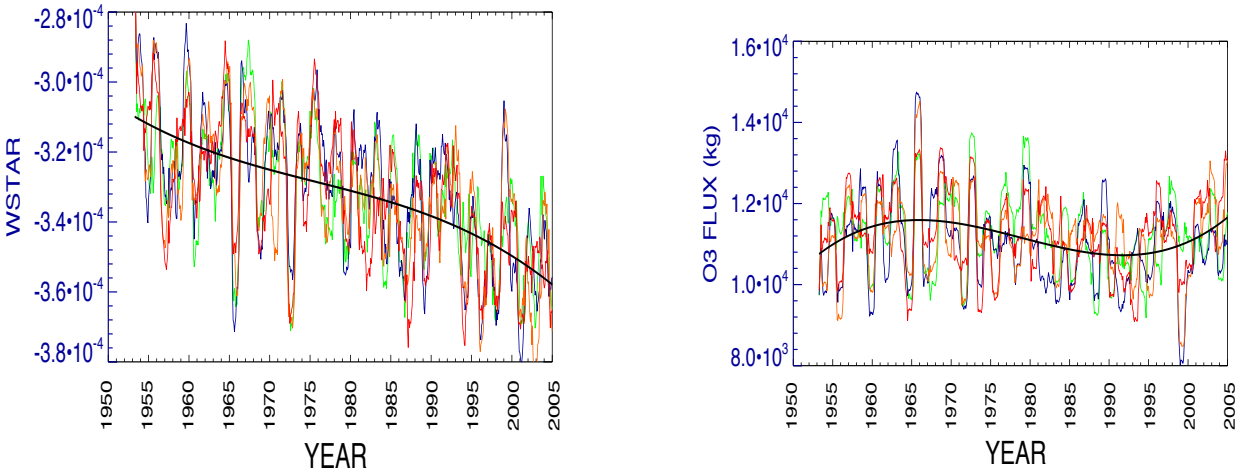

Figure 7:The (a) vertical residual velocity (w*, m/sec) and the (b) ozone flux (kg/year) averaged on the 150 hPa surface between 30 and 90^{o} N for each ensemble simulation (colored). The ensemble average fields are fit cubically and shown in black. A 12-month smoothing is used for all fields.

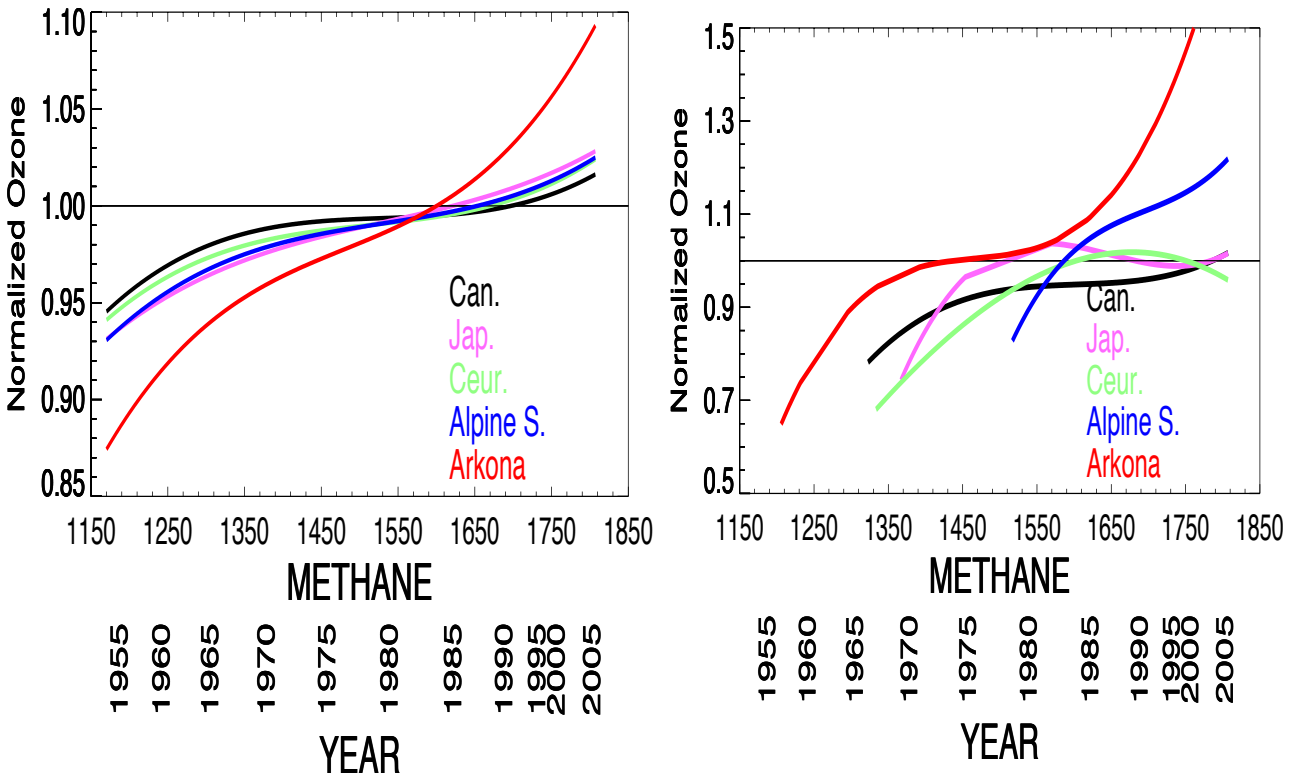

Figure 8: Simulated (left scale) and measured (right scale) cubic fits of normalized ensemble ozone versus global surface methane concentration for variouslong-term tropospheric measurement sites: The regional average of the Canadian (Can.), Central European (Ceur.) and Japanese (Jap.) ozonesonde sites at 500 hPa, the average of the JungfrauJoch and Zugspitze sites (Alpine S.) and the Arkona surface site. Ozone is normalized by its 1980-1985 concentration at each site. Globally averaged methane is from the WACCM simulation. The year corresponding to the methane concentration is given. Simulated ozone is the ensemble mean.

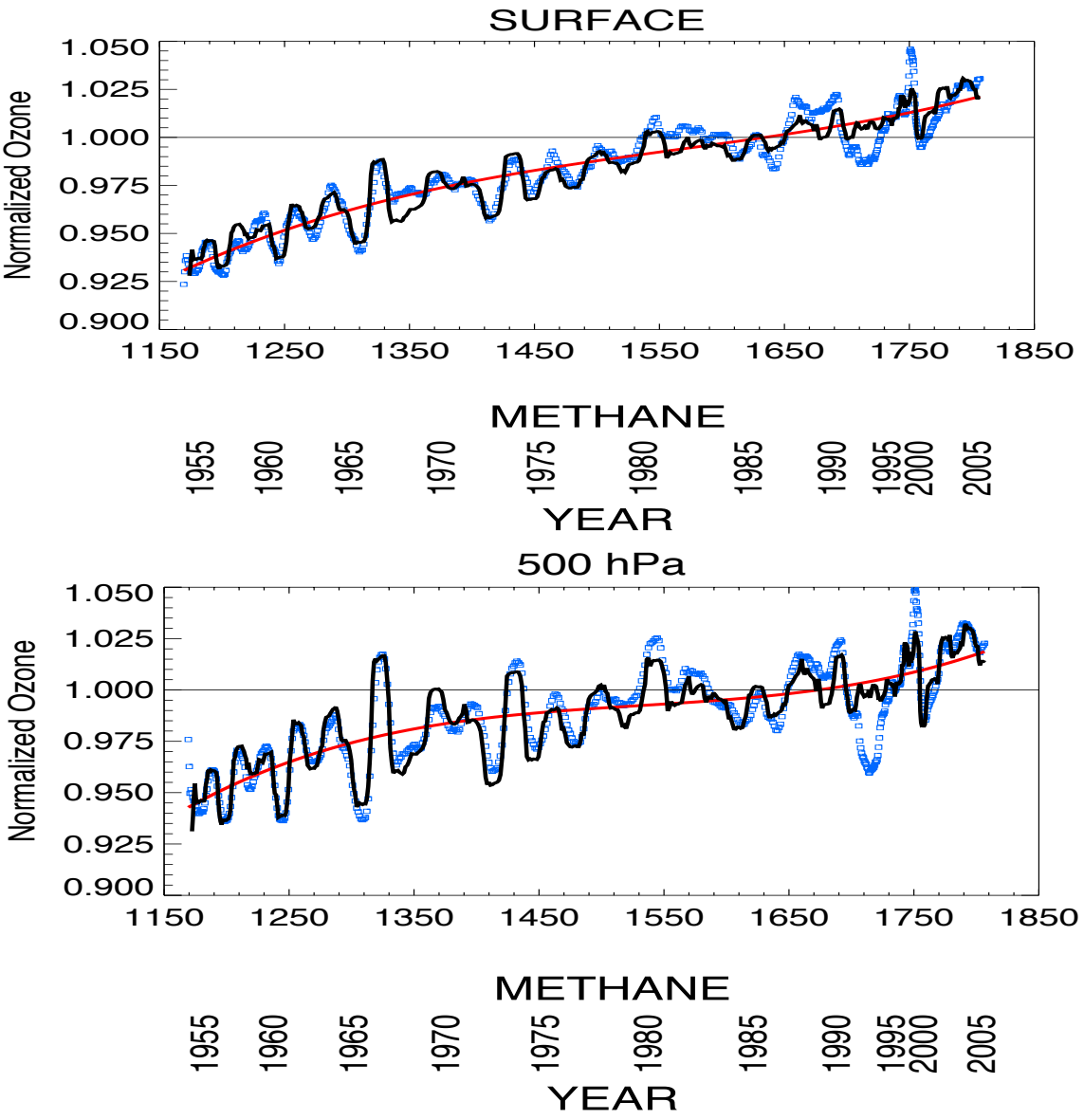

Figure 9: : Simulated (blue squares) normalized ozone and cubic fit (red line) and regressed fit (black line) to normalized ozone. Ozone is averaged from 30-90^{o} N at (a) the surface, (b) 500 hPa.

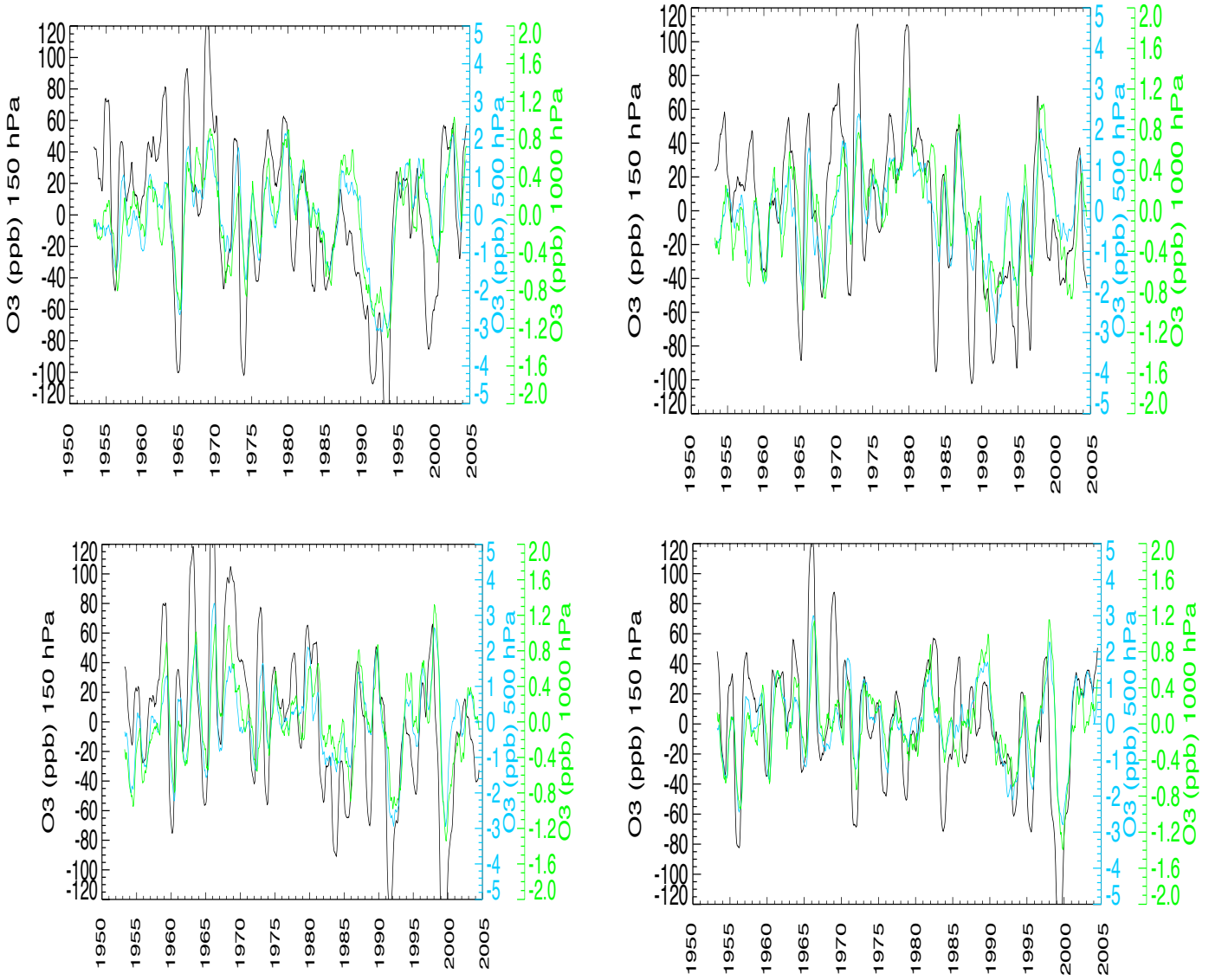

Figure 10: Ozone deviations (ppb) averaged from 30-90^{o} N for each of the four WACCM ensemble members at 150 hPa (black), 500 hPa (blue) and the surface hPa (green). The linear dependence on global methane has been removed from the ozone records at 500 and 1000 hPa. Monthly ozone deviations are smoothed over 12-months. Deviations are from ozone averaged over the entire simulation.

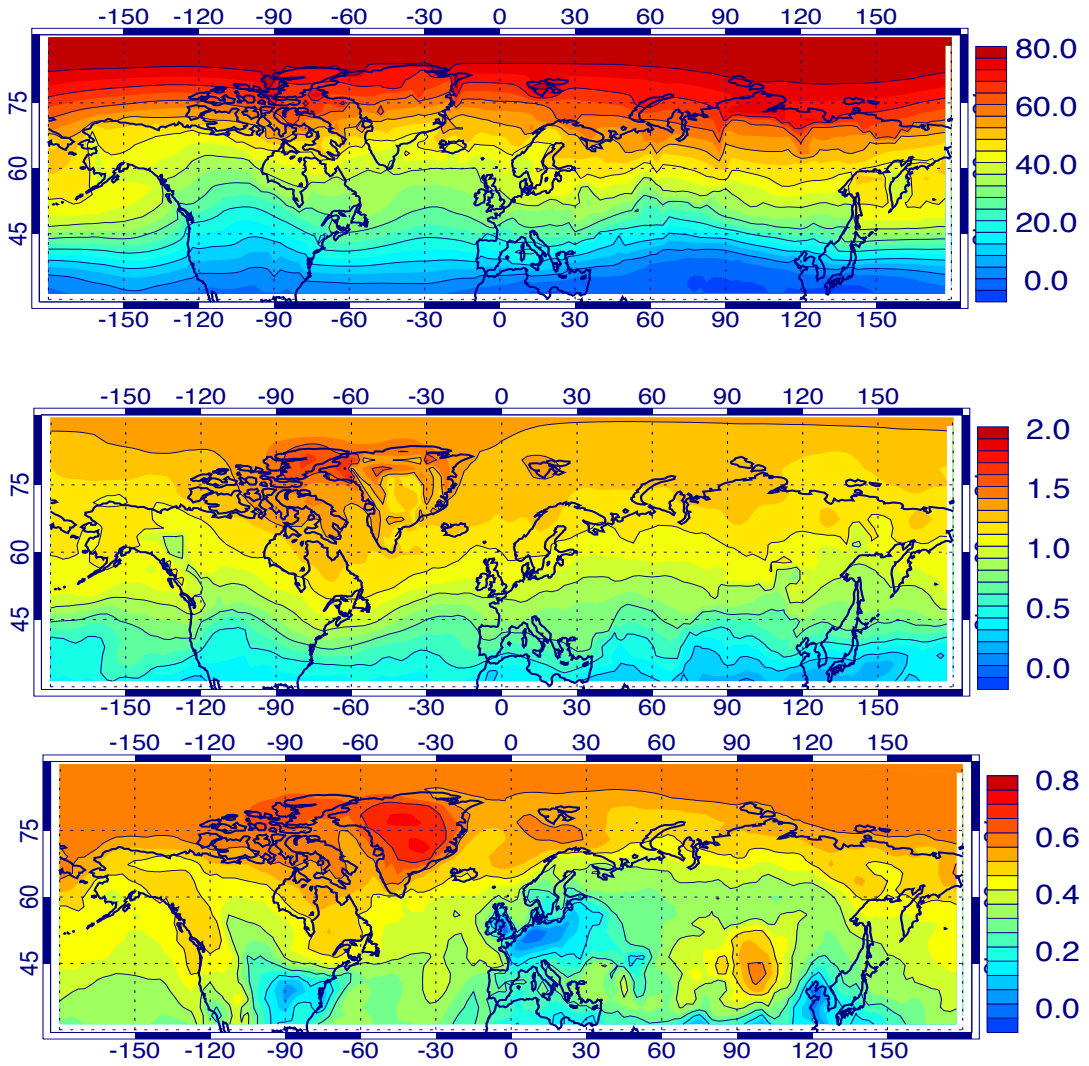

Fig11. Normalized first EOF component of detrended ozone at a) 150 hPa, b) 500 hPa and c) surface. Shown is the average for all four ensembles of the EOF multiplied by the standard deviation of the principal component. The absolute value of the result shows variability of ozone (ppb) expected due to variations in the first EOF component, the sign of the result shows the relation between variability in different locations.

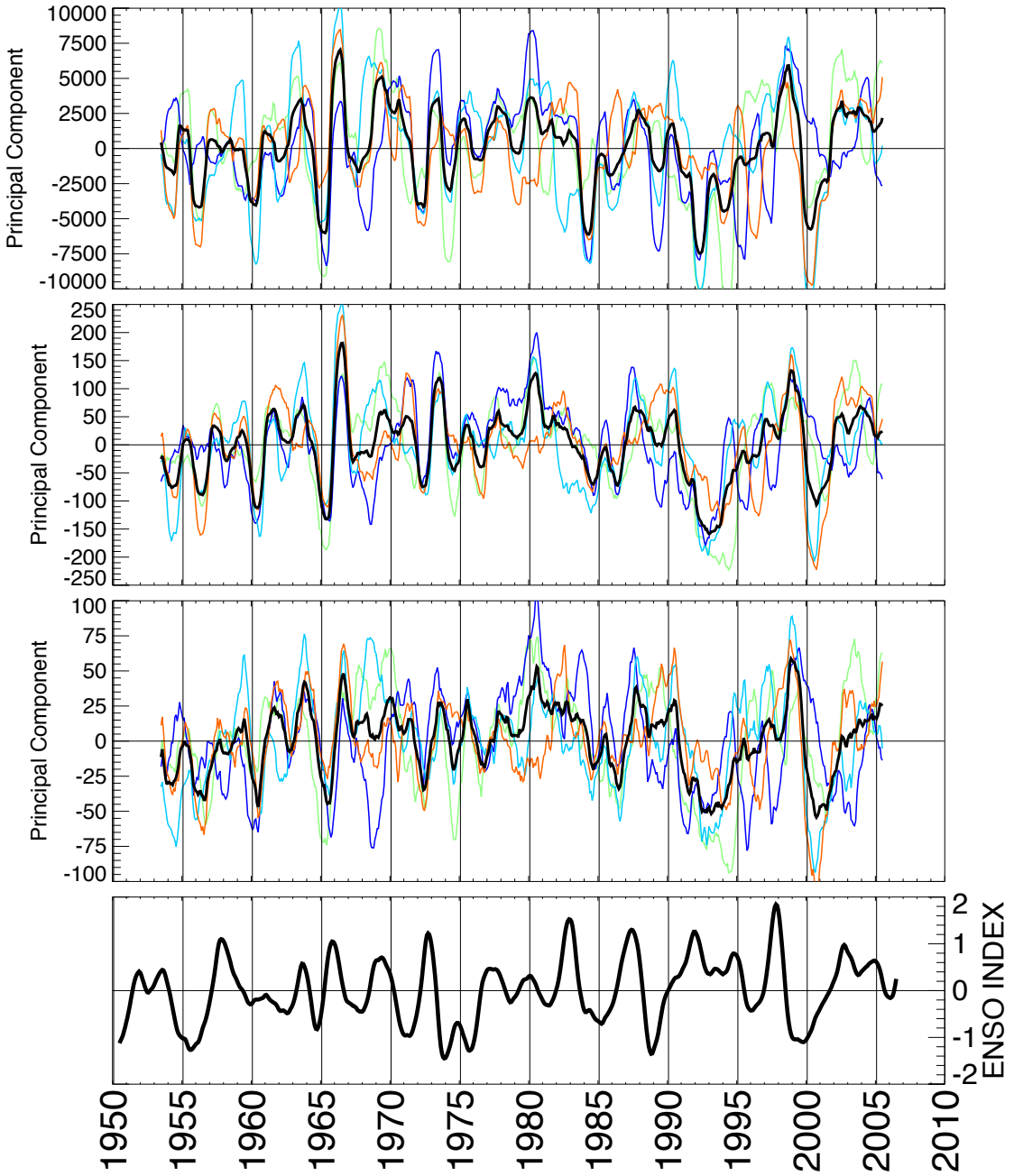

Fig. 12 Timeseries of the principal component for the first EOF of ozone from 30-90° N. for each ensemble simulation (color) and for ensemble mean (black) at 150 hPa (top panel), 500 hPa (second panel) and surface (third panel); ENSO index, lower panel.

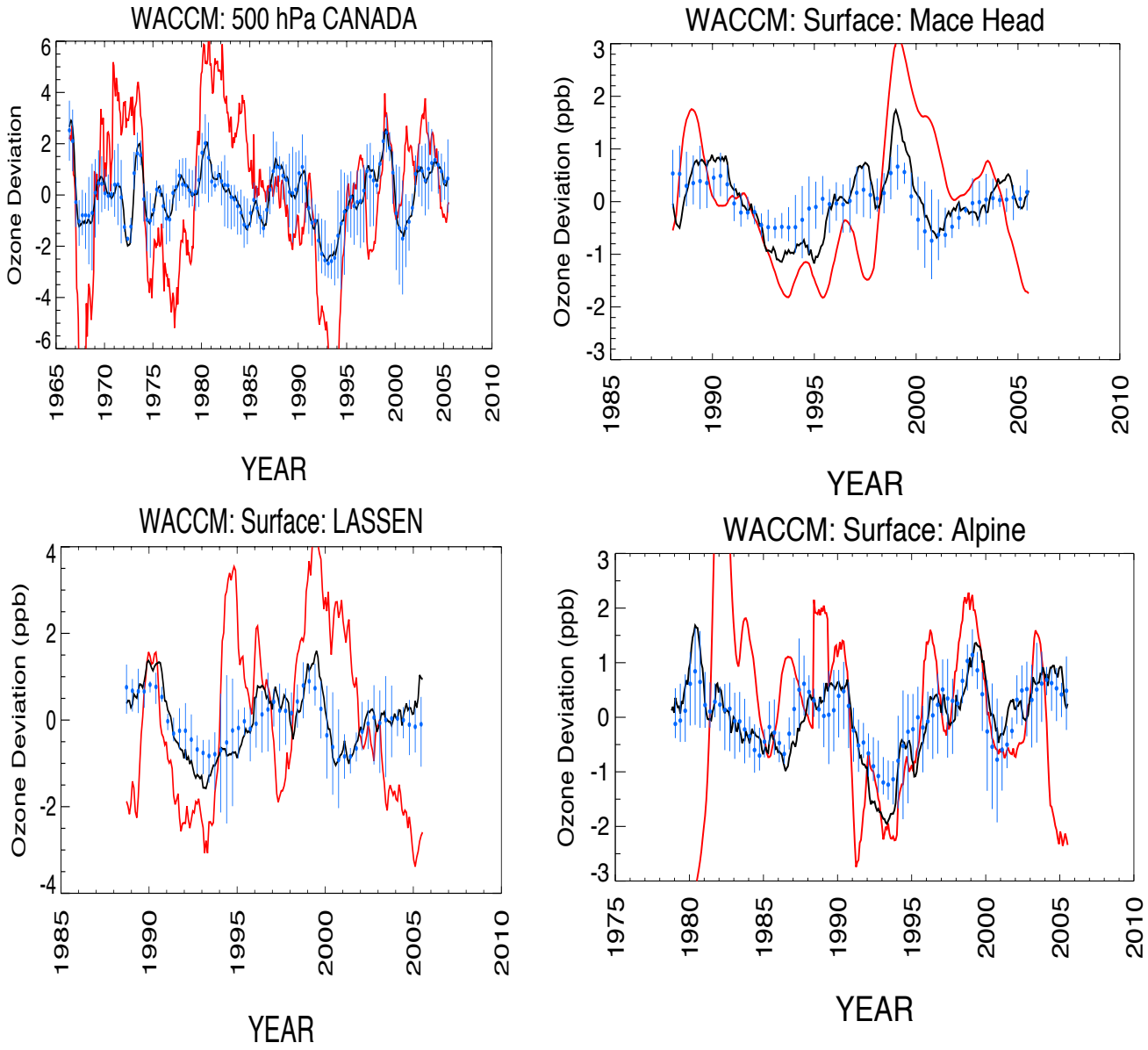

Figure 13. 12-month smoothed ozone deviations (ppb) for 500 hPa Canadian ozonesondes, Mace Head, Lassen, and the European alpine sites (note different scales in each figure): detrended measurements (red), ensemble average detrended ozone (black), the time variation of the EOF (blue), where the vertical blue lines bracket the range of the EOF over the ensemble members and the blue dot gives the ensemble average EOF. In each case ozone deviations are detrended against globally averaged methane over the common range of simulated and measured ozone.